2009

Assessment of depth of case-hardening in steel rods by electromagnetic methods

Chongxue Zhang
Iowa State University

Assessment of depth of case-hardening in steel rods by electromagnetic methods

by

Chongxue Zhang

A thesis submitted to the graduate faculty

in partial fulfillment of the requirements for the degree of

MASTER OF SCIENCE

Major: Electrical Engineering

Program of Study Committee:
Nicola Bowler, Major Professor
Jiming Song
Bruce Thompson

Iowa State University

Ames, Iowa

2009

TABLE OF CONTENTS

LIST OF TABLES

LIST OF FIGURES

ABSTRACT

Case depth measurements of surface hardened steel parts are important for quality control. The magnetic properties, including initial permeability, differential permeability and saturation magnetization of a series of induction-hardened and carburized steel rods were studied through measurements, with the aim of developing new methods to evaluate the case depth nondestructively. Four-point alternating current potential drop (ACPD) method also has the potential to evaluate different case depths. The potential drop was measured on a series of 1" diameter induction-hardened and carburized steel rod samples using a co-linear probe with pins aligned parallel to the axis of the rod.

For comparison with the above-mentioned electromagnetic measurements, hardness profiles were obtained by microhardness measurements.

It seems that measurements of initial permeability on surface hardened rods do not give a clear indication of case depth. Differential permeability was plotted versus applied magnetic field H. It is interesting to see that, when H is around 18 Oe, the differential permeability increases more-or-less in the sequence of case depth d in induction hardened samples. Differential permeability measurements give a good indication of case depth in induction hardened rods, but not carburized rods. The saturation magnetization decreases as the case depth increases. It was shown that four-point ACPD is a promising technique for distinguishing between different depths of case hardening. Especially in the low-frequency range of the real part of the normalized impedance, there is very good distinction between the case depths of the samples.

CHAPTER 1. OVERVIEW

Case hardening, or surface hardening, is a process which includes techniques used to improve the wear resistance of metal (often low-carbon steel) parts by hardening the surface without influencing the softer core. The combination of strength at the surface and ductility at the core is useful in parts like camshafts that must be very hard on the outside to resist wear but softer inside to resist impact produced in operation.

The conductivity and permeability of steel will change during the case hardening process. Therefore, case depth can be evaluated nondestructively by detecting the difference of the electric and/or magnetic characteristic using the electromagnetic methods [1].

1.1 Motivation

Compared to no treatment, case hardening increases the service life of components. Case hardening has advantages over through-hardening because it reduces heat treatment cycle time and cost. Also, case hardening is used on low-carbon steel which is less expensive than medium and high-carbon steels, while the through-hardening process is used on medium and high carbon steels.

Moreover, case hardening reduces cost of time and energy by treating only the surface area and limited inner area while through hardening treats the entire part.

Case depth measurements are important for quality control of surface-hardened steel parts and the heat treating process. The standard method of determining case depth is the microhardness test, in which indentions are made from the surface to the core of polished samples to determine the corresponding hardness values. This method is destructive and time consuming. There have been many efforts to evaluate the hardness and case depth using new

methods, which include magnetic characterization, four-point probes and image processing. In this thesis, magnetic properties including initial permeability and differential permeability, as well as saturation magnetization of case hardened steel rods were studied to evaluate the case depth. Four-point ACPD measurements were also made on the surface-hardened samples for case depth evaluation.

1.2 Case hardening process

In order to improve both the wear resistance and the fatigue strength of steel components under dynamic and/or thermal stresses, parts are often subject to the process of case hardening, which makes the surface layer, known as the case, significantly harder than the residual material, known as the core. Case hardening methods include induction-hardening, carburizing, nitriding, carbonitriding, cyaniding and flame hardening. Chemical composition, mechanical properties, or both are affected by the process. Case hardness depth, or the thickness of the hardened layer, is an important quality attribute of the case hardening process.

The microstructure of steel changes during the case hardening process. The untreated steels are two phase mixture of α-Fe (ferrite) and Fe_3C (cementite) as can be seen from Figure 1.1. The crystal structure of ferrite is body centered cubic (BCC). A typical heat treatment usually starts with an austenitization treatment where the ferrite (α-Fe, BCC) phase transforms to the austenite (γ-Fe, FCC) and all carbides are dissolved in the austenite. The temperature of the austenitization treatment varies for different steels but usually is in the range $1500°F - -1900°F$.

The microstructure of the case is transformed to martensite to achieve higher hardness values. Martensite is a single-phase structure that is formed when austenitized iron-carbon alloys are rapidly cooled (or quenched) to a relatively low temperature [2]. The martensitic transformation occurs when the quenching rate is rapid enough to prevent carbon diffusion. Ferrite and cementite phases will form if diffusion occurs.

Induction-hardened and carburized samples are studied through this thesis, so the induction hardening and carburizing process will be introduced in the next few paragraphs.

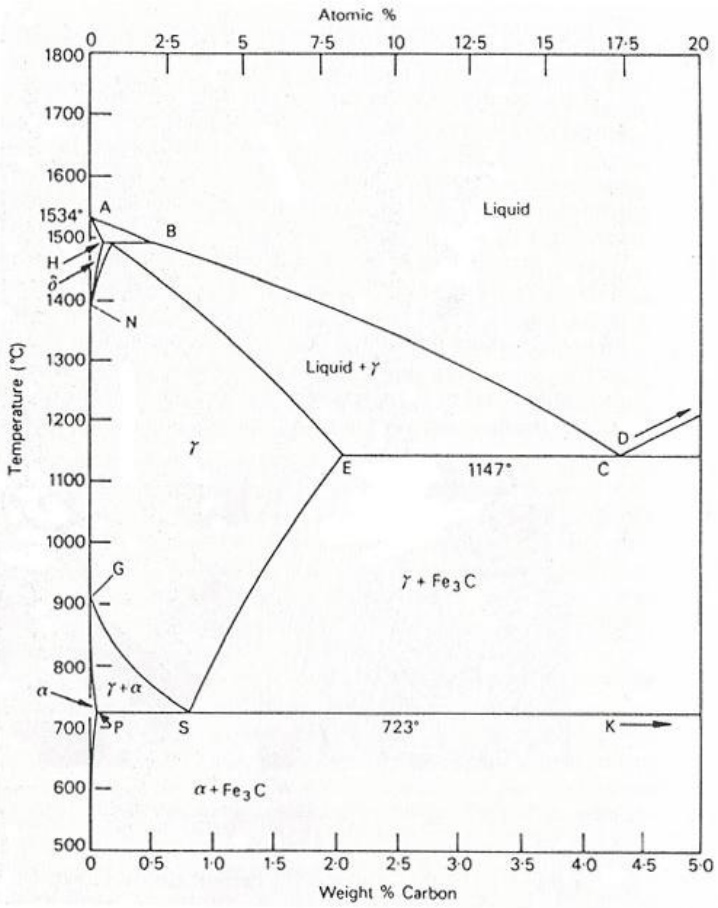

Figure 1.1 Iron carbon phase diagram (Source: [3])

1.2.1 Induction hardening

Induction hardening is widely used for the surface hardening of steel parts. The components are heated by electromagnetic induction to a temperature within or above the transformation range and then quenched. High frequency alternating current is passed through an electromagnet of the induction heater, which induces eddy currents in the work piece. The induced current flow within the work piece is most intense on the surface, and decays rapidly below the surface. The outside will heat more quickly than the inside. The core of the sample remains unaffected by the treatment and its physical properties are the same as those of the bar from which it was machined while the case undergoes a martensitic transformation, which increases the hardness and brittleness of the part.

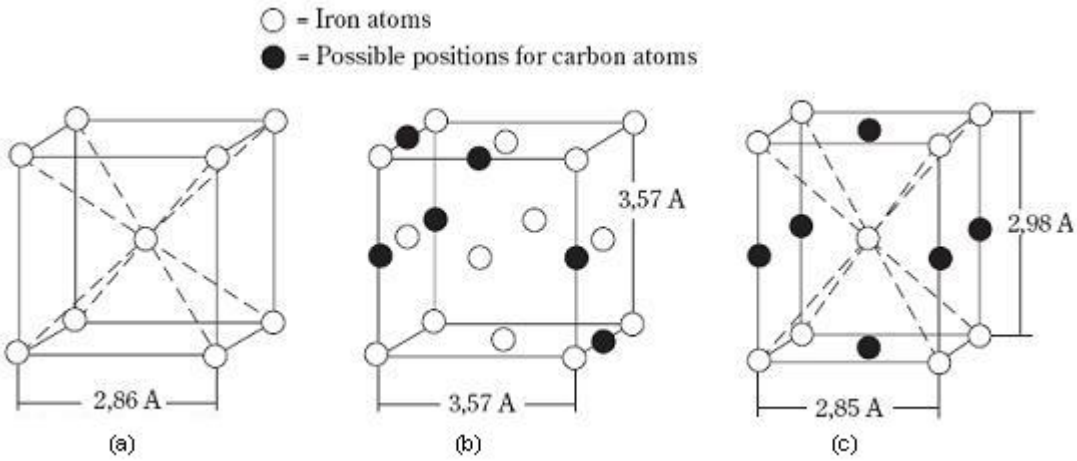

Figure 1.2 Crystal structure. (a) Unit cell in a ferrite crystal. Body–centered cubic (BCC). (b) Unit cell in an austenite crystal. Face-centered cubic (FCC). (c) Unit cell in a martensite crystal. Body-centered tetragonal (BCT). (Source: [4])

1.2.2 Carburizing

Carburizing is a case hardening process which adds carbon to the surface of low carbon steels (generally have base carbon contents of about 0.2% at temperatures between 850 and 950°C (1560 and 1740°F) to get high carbon austenite surface layer. After that the components are quenched to form the high carbon martensite case that is more wear and fatigue resistant. Case hardness of carburized components is primarily decided by carbon content while the case depth of carburized steel is a function of carburizing time and the available carbon potential at the surface. The carbon content of the case is usually controlled at between 0.8% and 1% and the surface carbon is often limited to 0.9% to avoid retained austenite and brittle martensite. Carburizing methods introduce carbon by using gas (atmospheric-gas, plasma, and vacuum carburizing), liquids (salt bath carburizing) or solids (pack carburizing).

1.3 Review of case depth measurement methods

The magnetic hysteresis properties and Barkhausen effect (BE) signals were studied in [5] to evaluate the case depth of a series of induction-hardened AISI 1045 steel rods. It was

assumed that the case depth is uniform and the induction signal from the entire rod $B_{rod}(H)$ is the sum of the induction of the case $B_{case}(H)$ and that of the core $B_{core}(H)$ weighed by the corresponding volume fractions:

$$B_{rod}(H) = V_c \times B_{case}(H) + (1 - V_c) \times B_{core}(H), \tag{1.1}$$

where V_c is the induction signal from the entire rod. $B_{core}(H)$ and $B_{case}(H)$ were measured from strip samples that were cut from the core and the surface layer of the hardened steel rods. After finding V_c from the above equation, the case depth d_c vas evaluated from by

$$d_c = \frac{1}{2} D(1 - \sqrt{1 - V_c}), \tag{1.2}$$

where D is the diameter of the steel rods. For samples with nominal case depth of 1.03, 1.45 and 1.95 mm, the percentage difference between the midpoint of hardness depth profile and the estimated case depth is -3.3%, -3.6% and 0.6%.

The magnetic Barkhausen emission (BE) profiles of the case carburized G86200 and G33106 steel sample was studied in [6]. The ratio of the two Barkhausen peaks was correlated to the case depth. The study showed that the magnetic Barkhausen emission technique could be used to detect the case depth below 1 mm more accurately. For components with a deeper case depth, it is also possible to estimate the minimum remaining case depth after grinding operations.

Magnetoacoustic emission (MAE) refers to the generation of elastic waves in ferromagnetic materials subjected to a magnetic field. MAE can be regarded as a complementary technique to BE, since MAE arises only from non-180° domain wall processes while BE is more sensitive to 180° domain wall processes [7]. MAE measurements were made on ten rods and plates of EN3B steel that were case-hardened by carbo-nitriding in [8]. The case depth thickness was determined from the frequency dependence of MAE. For plates, linear correlation was observed when measurements of the MAE I peak and area data were plotted versus the square root of the frequency. Single curves of gradient of the MAE I peak and area data versus case thickness could be developed. An accuracy of 10 percent for case depth less than 0.5mm and 20 percent for depths up to 2 mm was obtained.

Four-point direct current potential drop method was used to measure case depth in [9]. The experimental results confirmed that resistivity increases with hardening. The relationship between potential drop and case depth for various probe arrangement on surface hardened shaft like material with a diameter of 50 mm was analyzed. It was shown that the potential drop V increases while the increasing rate $\partial V/\partial d$ decreases with the case depth d.

Vibrational resonance spectra obtained with noncontacting electromagnetic-acoustic transducers (EMATs) were studied in reference [10] to determine the case depth of surface hardened steel shafts. A specific class of resonant modes were studied in 15.7-cm-long cut sections of sixty-three carbon steel shafts with various case depths. The measured resonant frequencies of the third mode were shown to be highly correlated with the 50 HRC case depth. For 63 shafts, the curve of 50 HRC depth versus the frequency of the third axial-shear mode was obtained by quadratic least squares fit to the data. The standard deviation of the fit is 0.13 mm on case depths of between 3 and 5.6 mm.

A quantitative calibrated technique based on photothermal radiometric (PTR) depth-profilometry for evaluating effective case depth in heat treated case-hardened steel products was demonstrated in [11]. Three types of heat-treated and carburized C1018 industrial steel screws with different case depths and screw heads (hexagonal, cylindrical and spherical) were evaluated. Correlation/calibration curves for each type of sample were established using conventional microhardness measurements. It was found that the PTR thermal-wave interferometric phase minimum determination method is suitable for evaluating case depths $\geq 300\mu m$ in this type of steel. It was shown that PTR phase minima can be used as a fast on-line inspection method of industrial steel products for quality control of industrial heat treating processes.

In another study, image processing was used to determine the case depth of the induction hardened steel JIS S 45 C, 20 mm in diameter and 15 mm in length [12]. The specimens were cut at a mid length, ground and etched with 10% nital and then scanned by a scanner. The scanned images were evaluated by identifying the gray level difference using a developed software. Compared to the microhardness test method, the developed method has a deviation

of ±0.12 mm at the case depth range of 0.6-2.0 mm and ±0.14 at the range of 2.1-4.3 mm. However, the program does not work when the steel was induction hardened more than once and it is not suitable to measure case depth of carburized part. Also, it is not a practical NDE option because it is essentially a destructive technique.

CHAPTER 2. SAMPLE FABRICATION AND CHARACTERIZATION

2.1 Fabrication

Two sets of steel rods, induction hardened 1" diameter 4140 steel rods and carburized 1" diameter 8620 steel rods were prepared. AISI/SAE 4140 is considered a high-strength, medium-carbon low-alloy steel [13]. Chemical compositions are given in Table 2.1. The steel 4140 is used for many high-strength machine parts (some of them nitrided) such as connecting rods, crankshafts and pump parts. AISI/SAE 8620 is a hardenable low alloy steel often used for carburizing to develop case-hardened parts. Its chemical composition ranges and limits are given in Table 2.2. In the carburized condition, this alloy is used for gears, shafts and crankshafts.

Table 2.1 Chemical compositions of 4140 steel (Source: [13])

Component	**Wt. %**
C	0.38-0.43
Mn	0.75-1.00
Si	0.20-0.35
Cr	0.80-1.10
Mo	0.15-0.25

Table 2.2 Chemical compositions of 8620 steel (Source: [13])

Component	**Wt. %**
C	0.17-0.23
Mn	0.60-0.90
Si	0.15-0.30
Cr	0.35-0.60
Mo	0.15-0.25
Ni	0.40-0.70

The Lot ID, case depth and measured precise diameter values of the induction-hardened sample set are provided in Table 2.3, while those for the carburized steel rods are given in Table 2.4. We have two samples for each treatment, marked by -1 and -2 in the induction hardened set, and by -A and -B in the carburized set. Processing information for the Induction hardened 1" diameter 4140 steel rods is provided in Table 2.5.

Table 2.3 Parameters of induction hardened 4140 steel rods. 7397-1 and 7397-2 are baseline samples, they are heated but not hardened. set1-1 and set1-2 are samples with no treatment. Measurement points for diameters are chosen along different lines parallel to the long axis of the rod.

Lot ID	**Nominal depth of hardening (mm)**	**Case depth measured by manufacturer (mm)**	**Diameter (mm)**
7393-1	0.75	0.724	25.6 ± 0.2
7393-2	0.75	0.724	25.8 ± 0.3
7394-1	1	1.008	25.9 ± 0.4
7394-2	1	1.008	26.1 ± 0.4
7395-1	2	2.075	26.0 ± 0.3
7395-2	2	2.075	26.4 ± 0.5
7396-1	3	3.071	26.3 ± 0.4
7396-2	3	3.071	26.5 ± 0.5
7397-1	0	0	26.6 ± 0.5
7397-2	0	0	26.6 ± 0.6
set1-1	0	0	26.1 ± 0.2
set1-2	0	0	26.0 ± 0.2

For carburized 1" diameter 8620 steel rods, all test rods were processed in Lindberg Pacemaker Integral Quench furnaces (information supplied by Drew Manning, Process Metallurgist, Advanced Heat Treat Corporation, Waterloo, IA). The atmosphere control in the furnaces uses a nitrogen/methanol base system with carbon control fluctuation with additional gases. The parts were loaded into the furnace vertically. After the heating cycle, the parts were quenched after the heating cycle in $140 - 160\,^{\circ}$F agitated oil. The parts were washed in a parts washer to remove any residual oil, and they were tempered at $300\,^{\circ}$F for 2 hours.

Lot ID 6803 (0.5 mm) was heated at $1700\,^{\circ}$F for approximately 2 hours at an approximate 1.0-wt% carbon potential. The parts were allowed to cool and equalize at $1550\,^{\circ}$F and an

Table 2.4 Parameters of carburized 8620 steel rods. 6840-A and 6840-B are baseline samples, they are heated but not hardened. set3-1 and set3-2 are samples with no treatment. Measurement points for diameters are chosen along one line parallel to the long axis of the rod.

Lot ID	**Nominal depth of hardening (mm)**	**Case depth measured by manufacturer (mm)**	**Diameter (mm)**
6803-A	0.5	0.609	25.2 ± 0.2
6803-B	0.5	0.609	25.1 ± 0.2
6804-A	0.75	0.78	24.2 ± 0.1
6804-B	0.75	0.78	25.2 ± 0.1
6805-A	1	1.128	25.1 ± 0.1
6805-B	1	1.128	25.2 ± 0.3
6807-A	1.5-2	1.6	25.0 ± 0.2
6807-B	1.5-2	1.6	25.0 ± 0.2
6840-A	0	0	25.0 ± 0.2
6840-B	0	0	25.3 ± 0.2
set3-1	0	0	25.6 ± 0.3
set3-2	0	0	26.1 ± 0.3

approximate 0.85-wt% carbon potential prior to quenching.

Lot ID 6804 (0.75 mm) was heated at 1700 °F for approximately 5 hours at an approximate 1.0-wt% carbon potential. The parts were allowed to cool and equalize at 1550 °F and an approximate 0.85-wt% carbon potential prior to quenching.

Lot ID 6805 (1.0 mm) was heated at 1700 °F for approximately 7.5 hours at an approximate 1.0-wt% carbon potential. The parts were allowed to cool and equalize at 1550 °F and an approximate 0.85-wt% carbon potential prior to quenching.

Lot ID 6807 (1.5-2.0 mm) was heated at 1725 °F for approximately 19 hours at an approximate 1.0-wt% carbon potential. The parts were allowed to cool and equalize at 1550 °F and an approximate 0.75-wt% carbon potential prior to quenching.

Lot ID 6840 (baseline) was completely masked with "Condursal 0090" stop-off paint (http://www.duffycompany.com/Condursal_0090.htm) to prevent carburization. The parts were then heated at 1700 °F for approximately 2 hours at an approximate 1.0-wt% carbon potential. The parts were allowed to cool and equalize at 1550 °F and an approximate 0.85-wt% carbon

Table 2.5 Processing information for induction hardened 1" diameter 4140 steel rods (information supplied by Drew Manning, Process Metallurgist, Advanced Heat Treat Corporation, Waterloo, IA).

	lot				
	7393	7394	7395	7396	7397
Nominal case depth 50 HRC (mm)	0.75	1.00	2.00	3.00	0.00 (temper only)
Induction machine					
Power rating (kW)	150	150	150	200	
Frequency rating (kHz)	30	30	30	10	
Quench					
Percentage*	5-7%	5-7%	5-7%	4-6%	
Pressure (PSI)	10	10	9-11	14-16	
Temperature (°F)	70-80	70-80	70-80	70-80	
Temper					
Time (hrs)	2	2	2	2	2
Temperature (°F)	300	300	300	300	300

potential prior to quenching (this should be a nearly identical heat cycle as Lot ID 6803). This method was utilized to best duplicate the core microstructure of the case hardened samples.

2.2 Hardness profiles

In order to make the microhardness measurements, samples were cut, mounted in bakelite, ground and polished, some polished samples are shown in Figure 2.1. Cylindrical samples 1/2" high were cut from the case hardened steel rods. Usually the edge tends to be polished more than the other part of the sample during the polishing process, thus samples were mounted to get better edge retention. The samples were polished starting from 600 GRIT, progressively down to 6 micron diamond paste and further to 3 micron aluminum paste. The surface smoothness was checked using optical microscope.

Microhardness profile measurements were made on both induction hardened rods and carburized rods using LECO LM247AT Microhardness Tester and Amh43 software. The indenter load used was 1000 g. Three measurements were made on each sample, along the direction of three diameters. One hardness profile for each induction hardened sample is presented in

Figure 2.1 Samples that were cut, mounted, ground and polished.

Figure 2.2, while hardness profiles of the carburized samples are shown in Figure 2.3.

The measured data t (depth) and y (Vickers hardness) was fitted using the following equation with two linear parameter c_1, c_2 and two nonlinear parameters λ_1, λ_2

$$y = c_1 \times \text{erfc}\left(\frac{t-\lambda_1}{\lambda_2}\right) + c_2, \tag{2.1}$$

where $\text{erfc}(x)$ is the complementary error function defined by

$$\text{erfc}(x) = \frac{2}{\sqrt{\pi}} \int_x^\infty e^{-t^2}\, dt. \tag{2.2}$$

λ_1 gives the profile midpoint, λ_2 is the transition width of the profile. $2c_1 + c_2$ determines the case hardness of the sample while c_2 represents the core hardness. The change in the shape of the fitted curve when c_1, c_2, λ_1 or λ_2 is changed is shown in Figure 2.4. In the Matlab code, we first guess initial values for λ_1 and λ_2, then use the complementary error function to calculate the complementary error. Then we do the least square regression analysis to estimate the linear parameters c_1 and c_2(to minimize the sum of the square error).The fitted curves for the induction hardened samples are given in Figure 2.5, while those for carburized samples are given in Figure 2.6.

The fitted parameters for the induction hardened steel rods are give in Table 2.6, while those for the carburized ones are given in Table 2.7. The fitted parameters shown are the average of three fitting results for each sample, based on the measured data along three different diameters when rotating the sample. The uncertainty is the standard deviation of three measurements. It

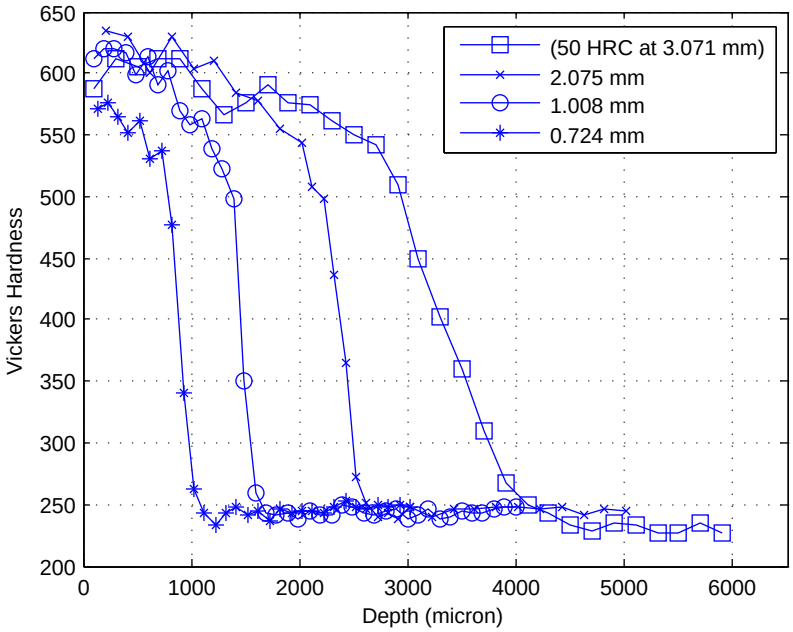

Figure 2.2 Hardness profiles of induction hardened samples

is shown that the fitting errors for carburized steel rods are smaller than those for induction-hardened sample. Complementary error function describes hardness profiles of carburized rods better than for induction-hardened rods. That is because case hardness of the induction-hardened sample is assumed to be constant during the fitting process, which is not true as can be seen from the hardness profiles.

Table 2.6 Fitted parameters for induction hardened steel rods with uncertainty obtained by comparing the results got from measurements along three different diameters when rotating the sample.

Sample	Case hardness (Hv)	Core hardness (Hv)	Fitting error (Hv)
7396	595 ± 10	224 ± 4	71 ± 12
7395	614 ± 12	241 ± 2	113 ± 29
7394	595 ± 4	242 ± 2	94 ± 6
7393	557 ± 2	245 ± 2	47 ± 6

Mid-hardness depth measured by curve fitting to microhardness profiles with uncertainties due to data scatter and rotation of rod is shown in Table 2.8 for induction-hardened rods

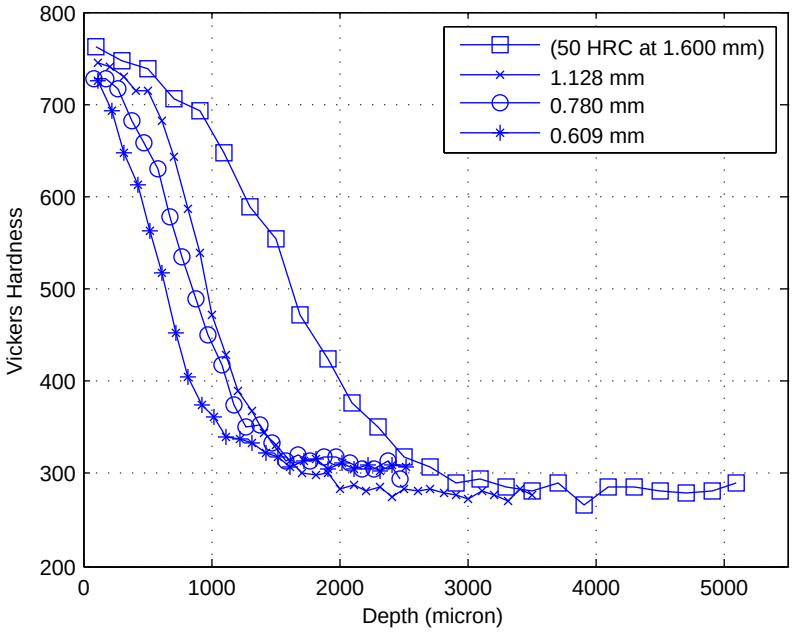

Figure 2.3 Hardness profiles of carburized samples

and in Table 2.9 for carburized rods. Uncertainty of the profile depth due to data scatter is calculated from

$$Uncertainty\ due\ to\ data\ scastter = Profile\ depth * Relative\ error, \tag{2.3}$$

where

$$Relative\ error = \frac{Fitting\ error}{Case\ hardness - Core\ hardness}. \tag{2.4}$$

Uncertainty of the profile depth due to rotation of the sample is the standard deviation of three

Table 2.7 Fitted parameters for carburized steel rods with uncertainty obtained by comparing the results got from measurements along three different diameters when rotating the sample.

Sample	Case hardness (Hv)	Core hardness (Hv)	Fitting error (Hv)
6807	759 ± 12	282 ± 4	36 ± 3
6805	758 ± 5	285 ± 3	50 ± 1
6804	752 ± 10	307 ± 8	32 ± 2
6803	801 ± 27	314 ± 6	36 ± 3

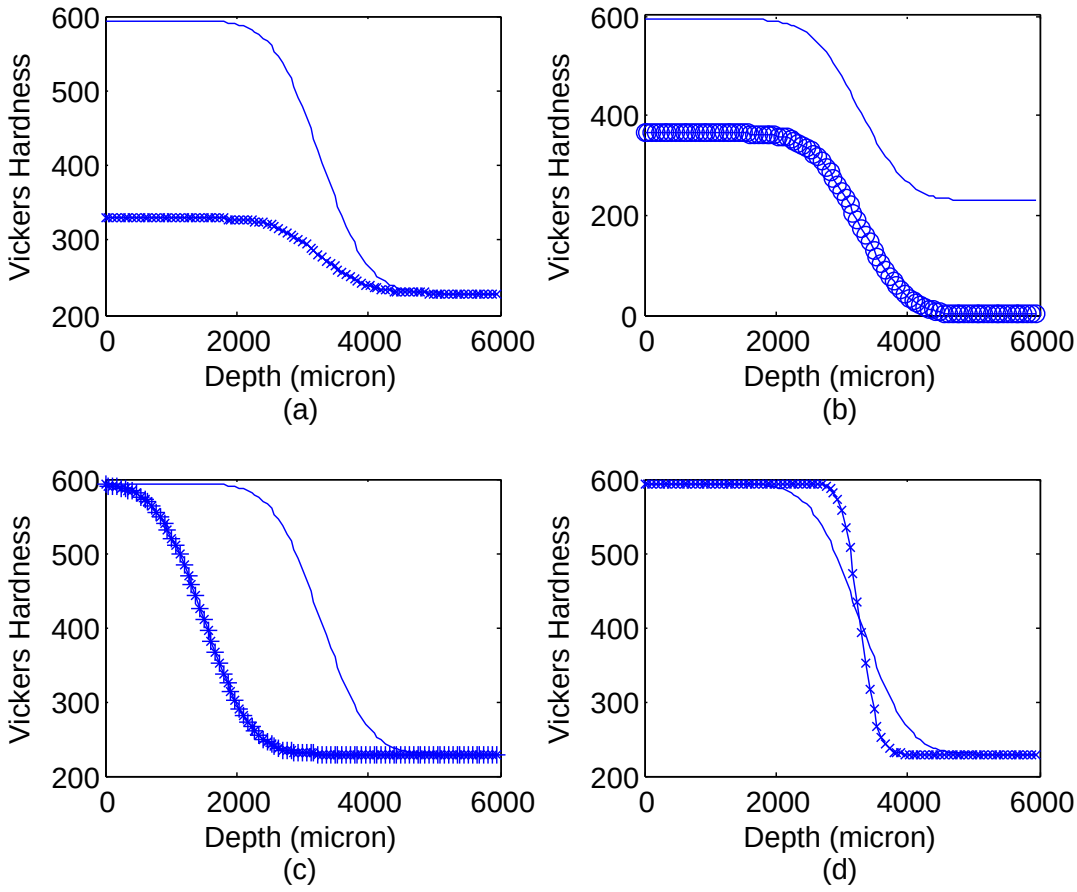

Figure 2.4 Fitted curve when $c_1 = 182$, $c_2 = 229$, $\lambda_1 = 3273$ and $\lambda_2 = 802$ compared with the curve when (a) c_1 is changed to 50, (b) c_2 is changed to 0, (c) λ_1 is changed to 1500, (d) λ_2 is changed to 300.

mid-profile depths got by fitting one curve for each data set of the sample. The uncertainty of the profile depth due to rotation of the rod is very small, which suggests that the case depth of a surface-hardened steel rod could be considered uniform. It is smaller than the uncertainty of profile depth due to scatter of data around fitted curve. Profile depth at 50 HRC is the value of the fitted profile depth that corresponds to 510 Hv, which is equal to 50 HRC in Rockwell unit.

Table 2.8 Case depths of induction hardened steel rods.

Sample	Profile depth with uncertainty due to data scatter	Profile depth with uncertainty due to the rotation of rod(mm)	Profile depth at 50 HRC (mm)	Manufacturer's depth at 50 HRC (mm)
7396	3.3 ± 0.6	3.30 ± 0.02	2.856	3.071
7395	2.3 ± 0.7	2.27 ± 0.04	2.175	2.075
7394	1.4 ± 0.4	1.43 ± 0.02	1.349	1.008
7393	0.9 ± 0.1	0.90 ± 0.04	0.805	0.724

Table 2.9 Case depths for carburized steel rods.

Sample	Profile depth with uncertainty due to data scatter	Profile depth with uncertainty due to the rotation of rod(mm)	Profile depth at 50 HRC (mm)	Manufacturer's depth at 50 HRC (mm)
6807	1.6 ± 0.1	1.58 ± 0.02	1.613	1.600
6805	1.0 ± 0.1	0.97 ± 0.01	0.981	1.128
6804	0.80 ± 0.06	0.80 ± 0.02	0.853	0.78
6803	0.54 ± 0.04	0.54 ± 0.02	0.632	0.609

2.3 Summary

In this chapter, the induction-hardened and carburized steel rods were described and hardness profiles of the samples were obtained. The chemical compositions, dimensions, processing information of the samples were provided as some background information. Hardness profiles were obtained by micro-hardness measurements in order to make a comparison with the electromagnetic measurements that will included in the next two chapters. The case depth, case hardness and core hardness of the samples were found by curve fitting to microhardness profiles and the uncertainties were analyzed.

In Chapter 3, the magnetic properties of the samples are studied to evaluate the case depth. In Chapter 4, Four-point alternating potential drop (ACPD) measurements on the surface-hardened samples are discussed.

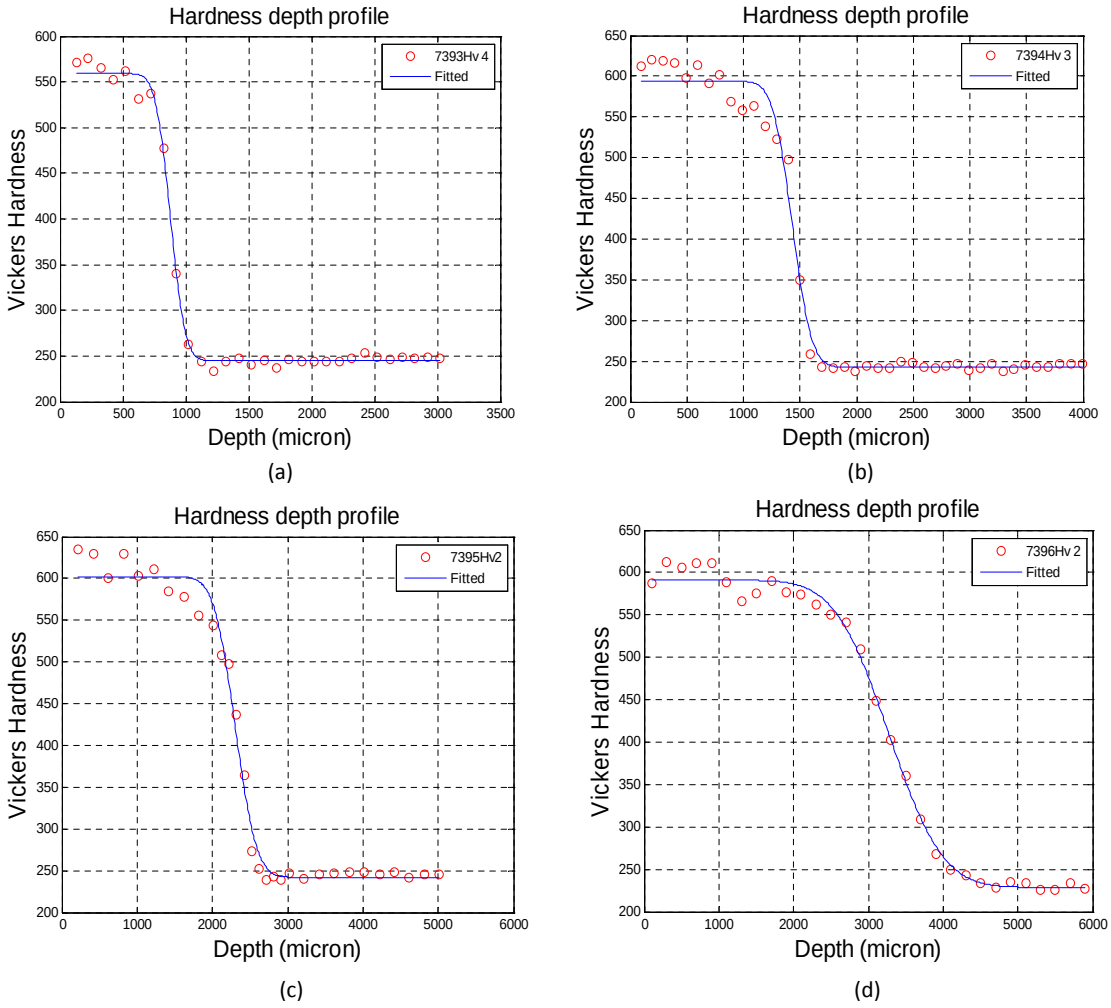

Figure 2.5 Fitted curves of induction hardened 1" diameter 4140 steel rods with nominal case depth of (a) 0.75 mm, (b) 1 mm, (c) 2 mm, (d) 3 mm.

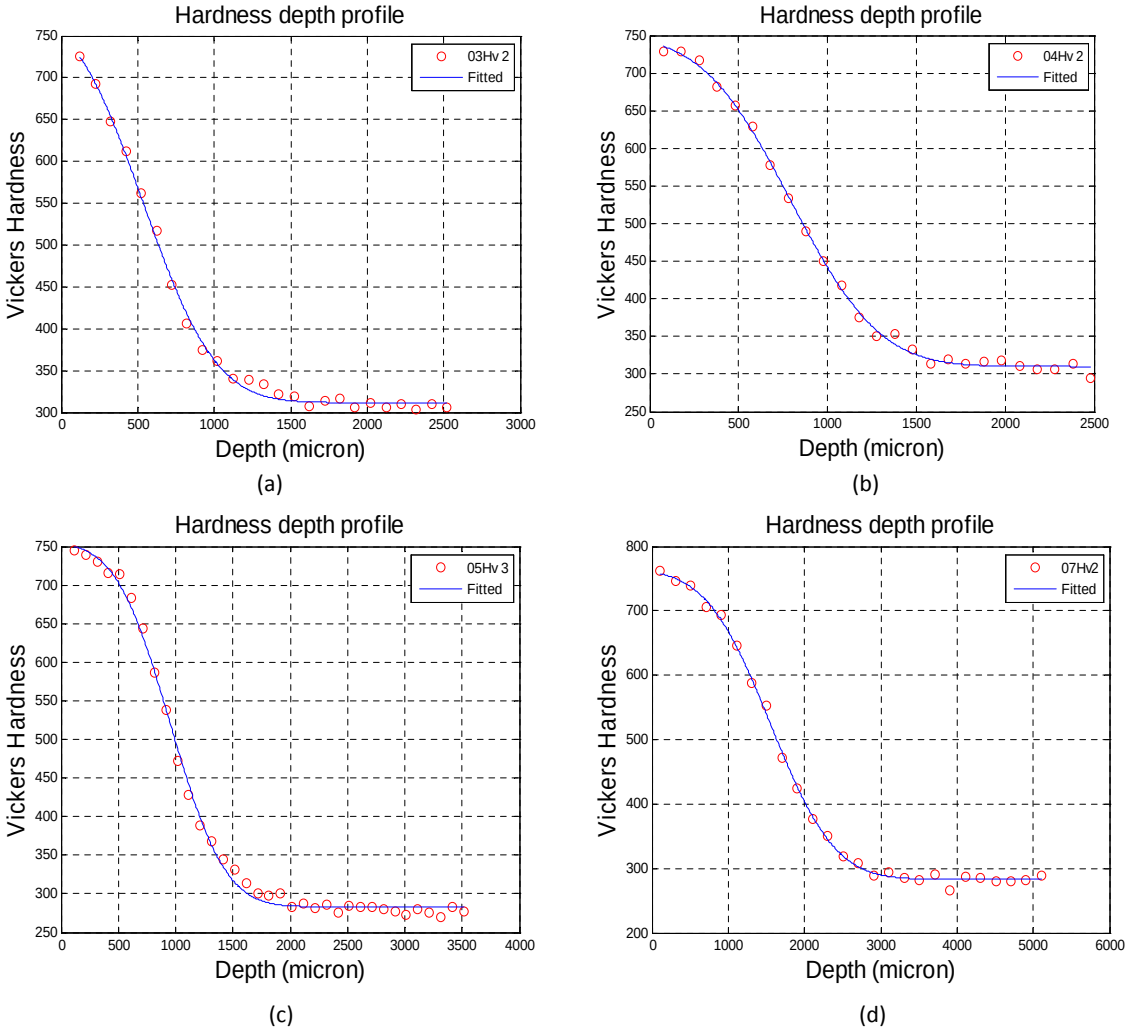

Figure 2.6 Fitted curves of carburized 1" diameter 8620 steel rods with nominal case depth of (a) 0.5 mm, (b) 0.75 mm, (c) 1 mm, (d) 1.5-2 mm.

CHAPTER 3. MAGNETIC TECHNIQUES

3.1 Introduction

The response of the ferro- or ferrimagnetic material when a magnetic field H is applied to it is called its magnetic induction B. The magnetic induction B is the same as the density of magnetic flux, Φ, inside the medium. So B is equal to the flux per unit area within a material. The plot of B versus H is called a hysteresis loop, or the B-H loop. A lot of information about magnetic properties of a material can be learned by studying its hysteresis loop. The hysteresis loop of a ferromagnetic material is shown in Figure 3.1 with several important parameters marked.

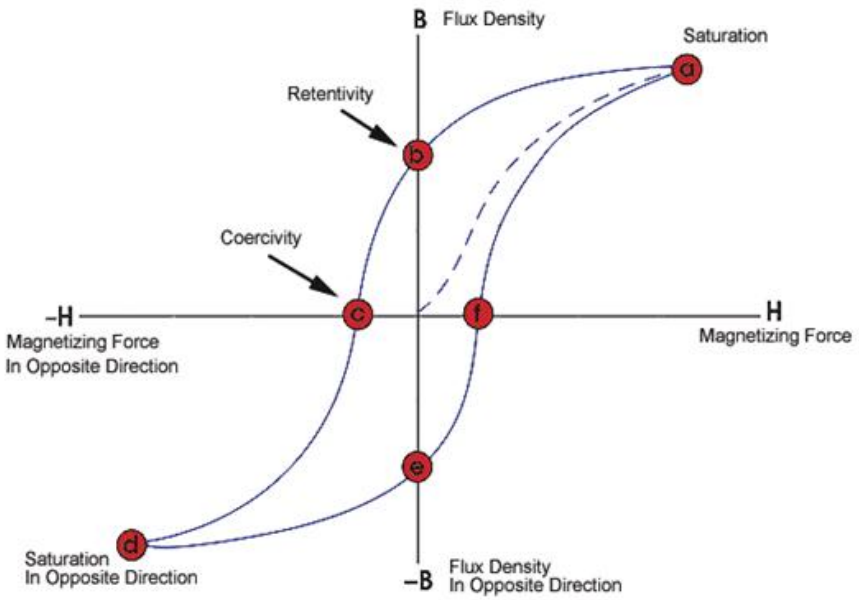

Figure 3.1 A hysteresis loop generated by measuring the magnetic flux of a ferromagnetic material when the applied magnetic field is changing. (Source: [14])

The value of B (point b) when H is reduced to zero after saturation is the retentivity, or the residual induction. The reversed H (point c) required to reduce B to zero is the coercivity. The permeability μ is the ratio of B to H. The initial permeability μ_i describes the permeability of a material at low values of B (below 0.1 T). Differential permeability is the slope of the B-H loop for a magnetic material, given by dB/dH.

In cgs units, the equation relating B and H is

$$B = H + 4\pi M, \tag{3.1}$$

where M is a property of the material, called the magnetization. The magnetization is defined to be the magnetic moment per unit volume.

$$M = \frac{m}{V}. \tag{3.2}$$

In the B-H plot for a ferri- and ferromagnetic material, the material starts at the origin in an unmagnetized state and B follows the curve from 0 to the saturation point as H is increased the in the positive direction. The valued of B at saturation is called the saturation induction B_s and the value of M at saturation is the saturation magnetization M_s. M is constant after saturation but B continues to increase because $B = H + 4\pi M$.

The magnetic properties, including initial permeability, differential permeability and saturation magnetization of the induction-hardened and carburized steel rods are studied in this chapter, with the aim of developing new methods to evaluate the case depth nondestructively.

3.2 Measurements of initial permeability

The initial permeability μ_i of case-hardened steel rods has been measured using a 'Magnescope'; a magnetic hysteresis measurement system developed in a collaborating DoE-sponsored program at Ames Laboratory, Iowa State University. The purpose of the measurements was to determine whether or not μ_i is strongly correlated with the depth of case hardening.

The Magnescope was used to demagnetize the samples and then plot the curves of magnetic induction B as a function of applied magnetic field H. The range of H used was -0.5 to 3 Oe, while the range of B measured was approximately -50 to 300 Gauss. μ_i was calculated by

fitting a second-order polynomial to the measured data. The polynomial used in the regression is $Y = A + B_1 * X + B_2 * X^2$, in which parameter B_1 represents μ_i. Several measurements were made on each sample to reduce the uncertainty in the measurements, as given in Table 3.1. The uncertainty listed is the standard derivation of μ_i got from each measurement, which gets smaller when the number of measurements gets bigger. One set of data obtained in this way on sample 7396-1 (detailed in Table 3.1) is shown in Figure 3.2.

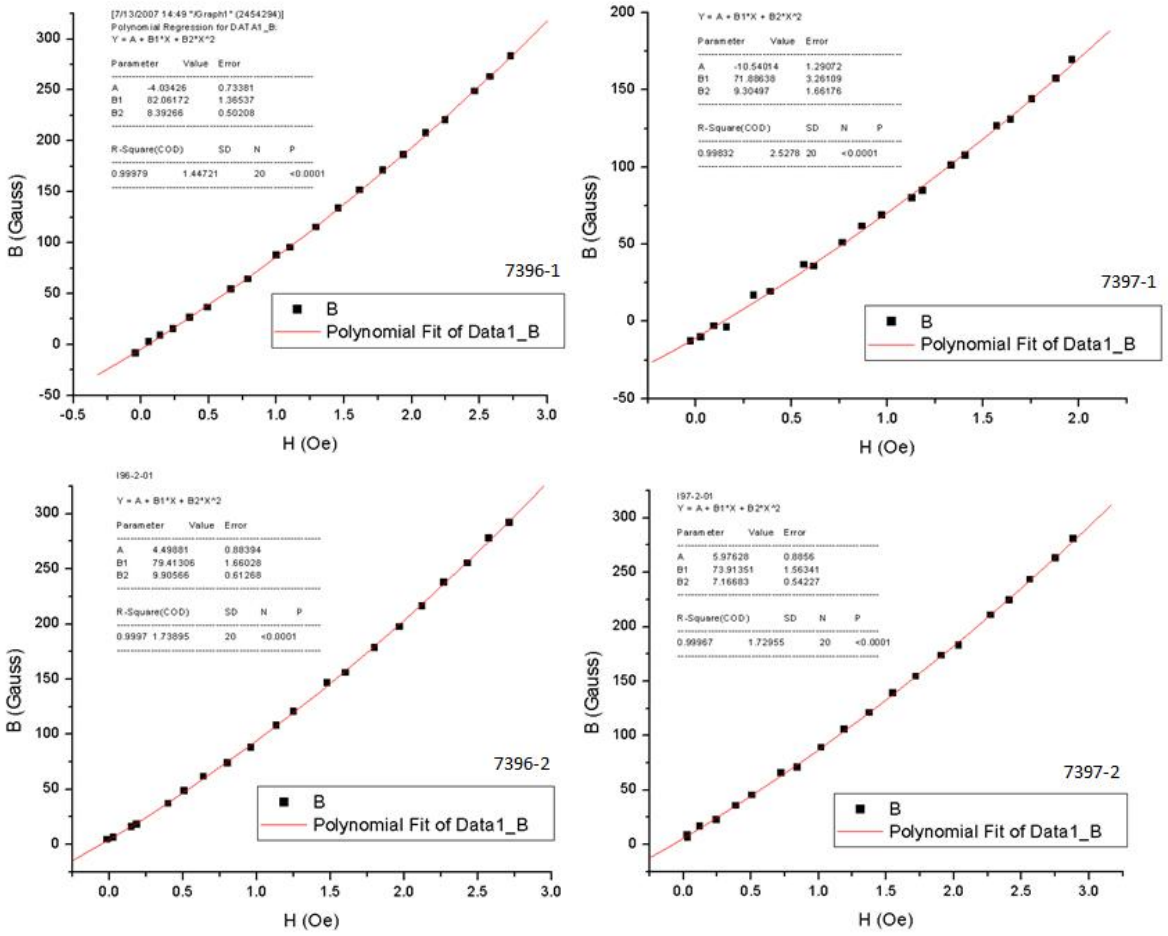

Figure 3.2 Example of finding μ_i by fitting a second order polynomial to the measured data for each sample.

Initial permeability measurements were made on 2 similar steel rod samples induction-hardened to depth 3.30 ± 0.02 mm, and 2 other similar rods that were heat treated but not hardened. The results are given in Table 3.1. The value of μ_i measured for the samples

Table 3.1 Measured initial permeability for surface-hardened and non-surface-hardened steel rods.

Sample	d (mm)	Average μ_i	No. of measurements	Data points in each curve
7396-1	3.30 ± 0.02	80 ± 5	5	20
7397-1	0	74 ± 3	5	20
7396-2	3.30 ± 0.02	80 ± 2	6	20
7397-2	0	73 ± 1	10	20

that were nominally the same agreed within experimental uncertainty. However, the contrast between values of μ_i measured for the surface-hardened and non-surface-hardened rods was not strong. In fact, even for the strong contrast in case depth considered in this study (0 mm compared with 3.30 mm), the values of μ_i obtained were not distinct when experimental uncertainty is taken in to account. It is concluded that μ_i is not a good indicator of case depth and for this reason μ_i of other samples is not studied.

3.3 Measurements of differential permeability

Hysteresis loop measurements were completed on the induction hardened and carburized 1" diameter steel rods. Magnetic field in the range of -130 Oe to 130 Oe was supplied by a solenoid driven by a Kepco power supply. The range of measured B was -23000 to 23000 Gauss. The sample was put into a plastic holder with inner diameter 2.61 cm and outer diameter 3.36 cm so that the sample is held in the center of the solenoid. The plastic holder is 46.23 cm long and it fits into the solenoid which is 54.36 cm long. A pick-up coil with 372 turns, which encircles the middle part the plastic holder, was used to measure the induction B. The magnetic field H is determined by the Hall sensor (In cgs, B and H are the same in the air) which is embedded in the middle of the plastic holder and contacts the surface of the sample directly (Figure 3.3). It was assumed that the direction of the magnetic field inside the middle part of the sample is parallel to the axis of the cylinder and B is uniform in the cross-section of the middle part. Because there is no surface electric current, the tangential components of the magnetic field are continuous due to the boundary conditions. Thus the magnetic field measured by the Hall sensor can be assumed to be the same as H inside the middle part of the sample.

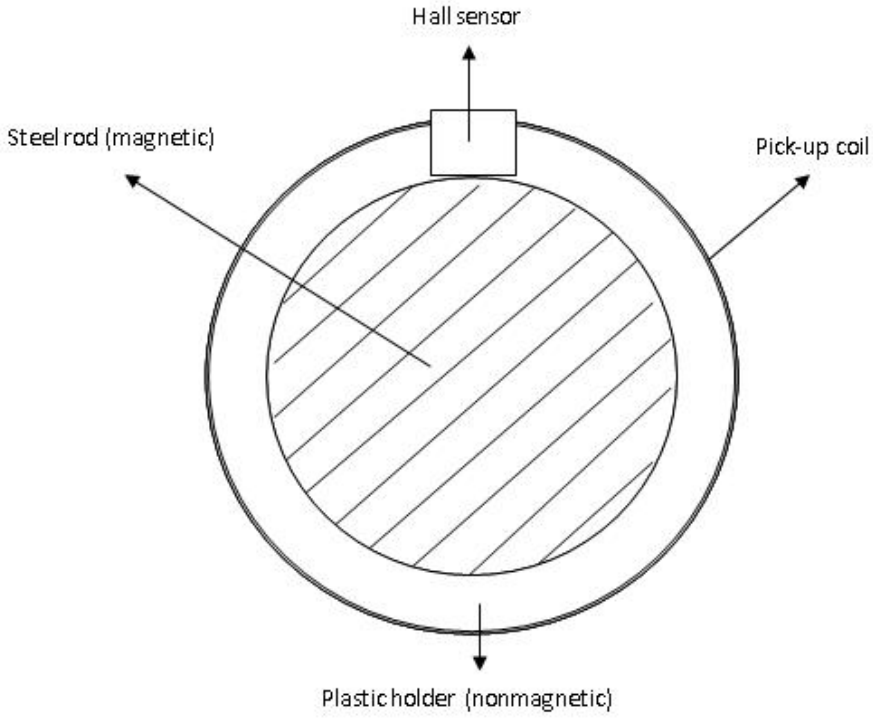

Figure 3.3 System set-up

Three hysteresis loops were measured on each sample, and the results averaged. The measured data was processed so that the loops were shifted slightly on the B-H axes so that their intercepts lay symmetrically about the zero point. This is common practice in analysis of hysteresis loops, to correct for instrumentation drift in the measurements (Another approach is to center the curves based on symmetry in their maximum values). Since the value of measured B depends on flux linkage ($B = \phi/A$, where ϕ is the magnetic flux and A is the cross-section area of the sample), values of B were corrected for minor differences in the cross-sectional area of the samples. The differential permeability, dB/dH, was calculated by finding the best fit straight line to a sequence of five data points and assigning the slope to be the differential permeability at the middle value of H.

Differential permeability is plotted versus H in the range of 0 to 30 Oe in Figure 3.4. It can be seen that, at around 18 Oe, there is a peak in dB/dH for the case-hardened samples that does not occur for the non-surface-hardened sample. This feature is shown in more detail in

Figure 3.5. It is interesting to see that, when H is around 18 Oe, the differential permeability increases more-or-less in the sequence of case depth d. The standard deviation in dB/dH, computed from the three sets of measured hysteresis loops, is of the order 10 Gauss/Oe, much less than the differences between dB/dH for the different samples. Figure 3.6 compares results for sample 7397-1, which is heated but not hardened, with those for sample 'set 1-1', which is 'as received' ie without any heat treatment at all. It can be seen that the differential permeability for these two rods is very similar.

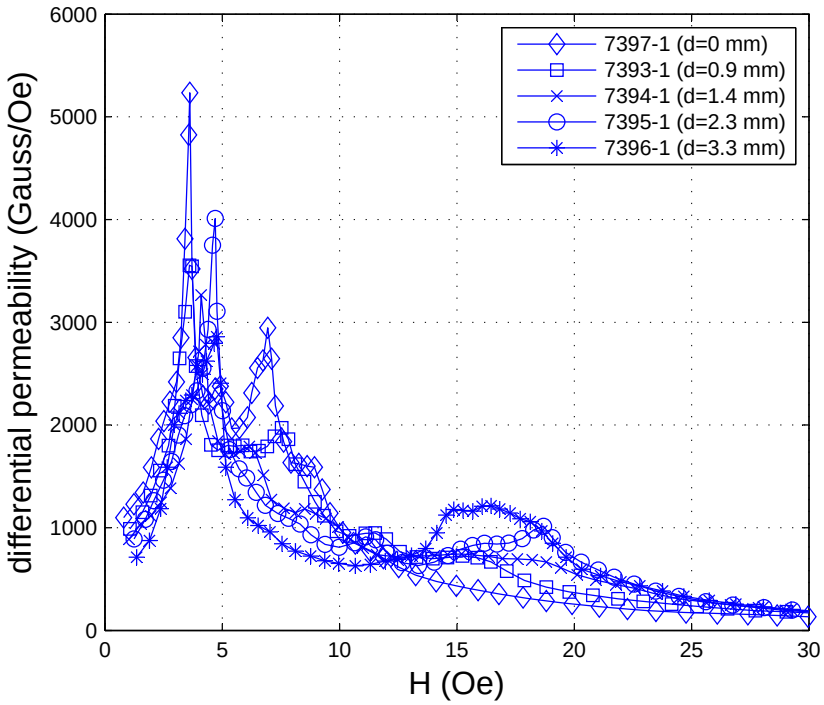

Figure 3.4 Differential permeability versus applied magnetic field for 1" induction-hardened steel rods with various values of case depth, d.

We have two samples for each case depth. Similar results are obtained for the second set as presented in Figure 3.4 to Figure 3.6 for induction hardened rods. The same measurements were performed on a set of carburized samples. The results are shown in Figure 3.7 to Figure 3.9. The feature in dB/dH that is seen clearly at around 18 Oe in the case of the induction-hardened samples (Figure 3.5) is visible in Figure 3.8 but is much weaker for these carburized specimens

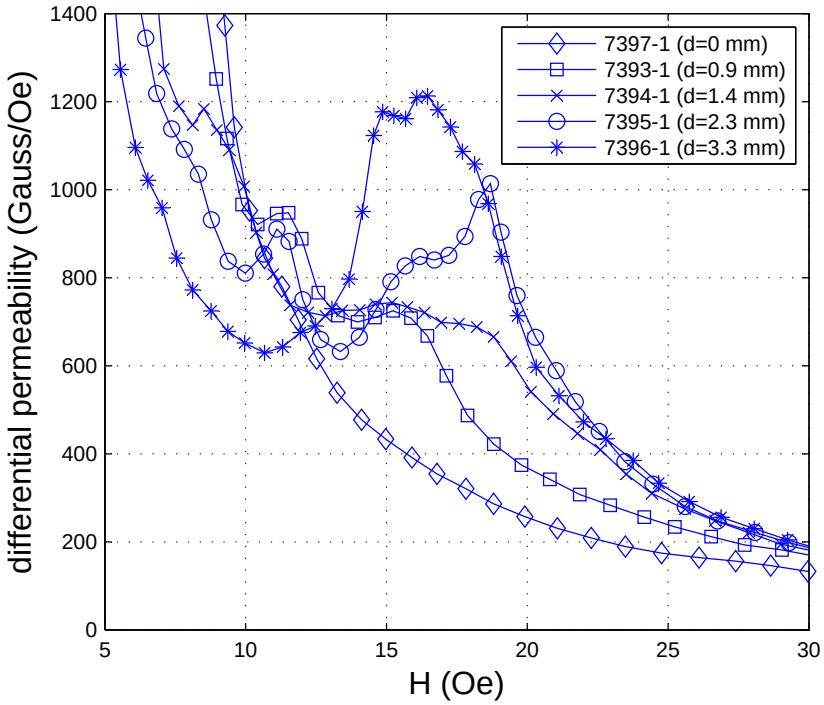

Figure 3.5 Differential permeability versus applied magnetic field for 1" induction-hardened steel rods with various values of case depth, d. The standard deviation in dB/dH, computed from the three sets of measured hysteresis loops, is of the order ±10 Gauss/Oe.

than for the induction-hardened specimens. Thus we conclude that it may be possible to use dB/dH as an indicator of case depth for induction-hardened specimens, but not for carburized specimens. Considering Figure 3.9 we also note that there is a large difference in dB/dH between untreated and heat-treated but not carburized 8620 steel rods, both of which have case depth $d = 0$. This is in contrast with observations on the untreated and heat-treated but not surface hardened 4140 steel rods, Figure 3.6, in which there is little difference in dB/dH between untreated and heat-treated but not surface hardened specimens. The observations indicate that 2-hour tempering of 4140 steel rods at 300 °F (specimen 7397-1) has little effect on the magnetic properties of the rods, whereas the heating to 1700 °F for 2 hours of the 8620 steel (to mimic heat treatment of the carburized rods, specimen 6840-A) effects a significant change on the magnetic properties of the rods.

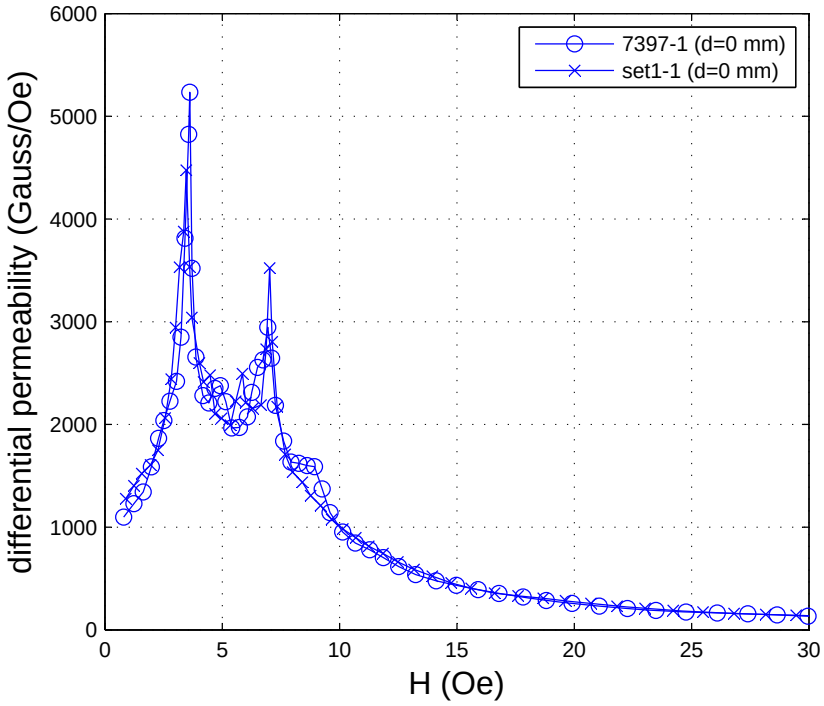

Figure 3.6 Differential permeability versus applied magnetic field for 1" 4140 steel rods with no surface hardening. Set1-1 is 'as received' and 7397-1 was heat treated but not surface hardened.

3.4 Measurements of Saturation Magnetization

3.4.1 Introduction

The magnetization M depends on both the individual magnetic moments of the constituent ions, atoms or molecules, and on how these dipole moments interact with each other [15]. The cgs unit of M is the emu/cm^3, the cgs unit of B is the gauss (G) and that of H is the Oersted (Oe). The saturation magnetization of pure iron at room temperature is 1714 emu/cm^3.

The magnetic field required to produce the saturation value varies with the relative geometry of H to the easy axes and other metallurgical conditions of the material [16]. The approach to saturation is a structure-sensitive process. Frölich established an empirical relation between M and H in 1881, since when several other empirical equations associated with the approach to saturation have been suggested. The ones proposed by Becker and Doring in

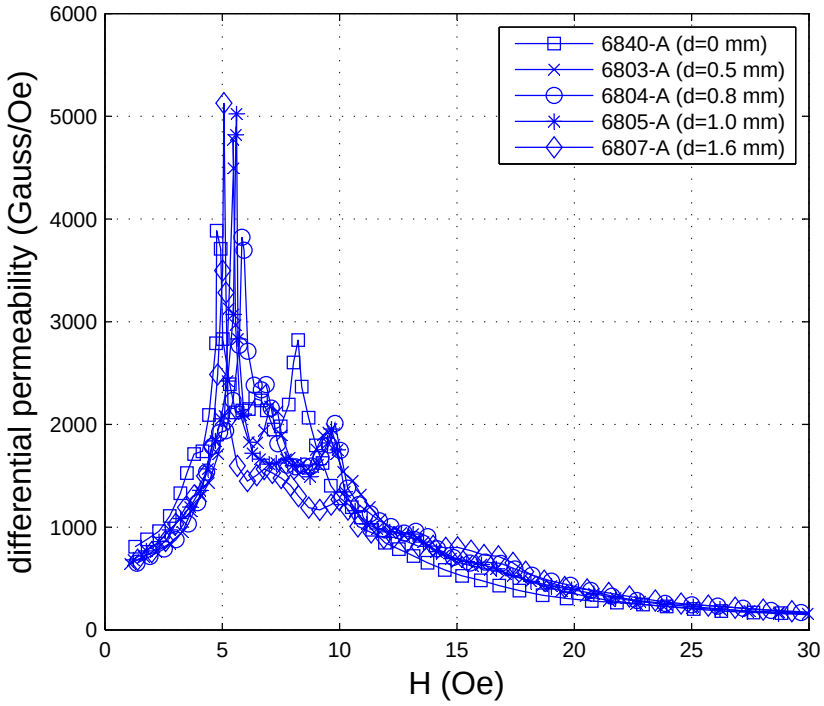

Figure 3.7 Differential permeability versus applied magnetic field for 1" carburized steel rods with various values of case depth, d.

1939 are considered most complete

$$M(T) = M_s(T)\left(1 - \frac{a}{H} - \frac{b}{H^2} - \cdots\right) + \chi_0 H, \tag{3.3}$$

$$M(0\,^\circ\mathrm{K}) = M_0\left(1 - \frac{a}{H} - \frac{b}{H^2} - \cdots\right), \tag{3.4}$$

where a, b, ... and χ_0 are constants.

It was shown in reference [16] that at the final stage of magnetization, we have the relation

$$M(T) = M_s(T)\left(1 - \frac{b}{H^2} - \cdots\right), \tag{3.5}$$

where T represents the temperature. So when M is plotted as a function of $1/H^2$, M_s can be found by fitting a polynomial to the plotted data.

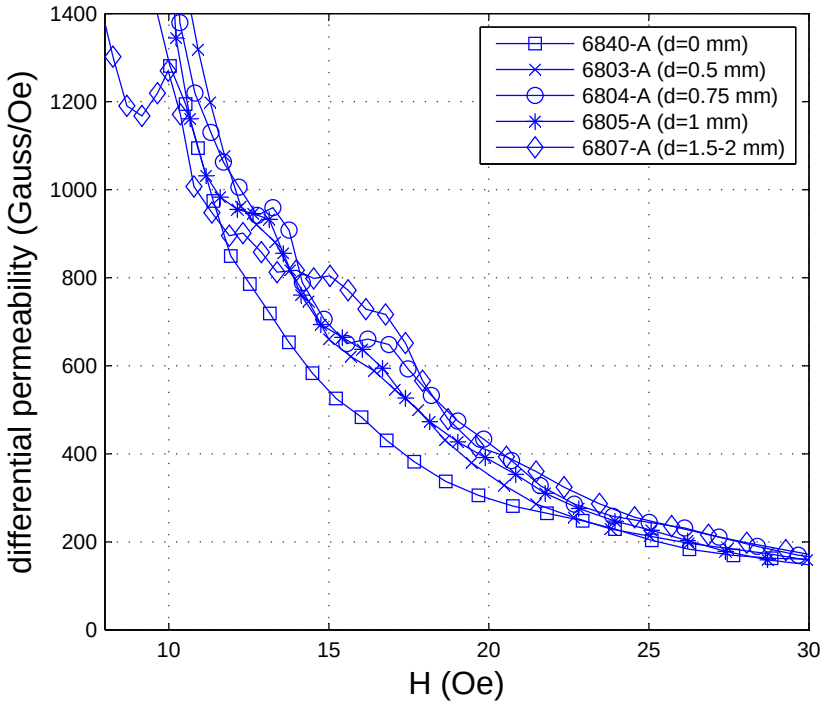

Figure 3.8 Differential permeability versus applied magnetic field for 1" steel rods with various values of case depth, d.

3.4.2 Modeling

The surface-hardened steel rod is modeled as a two layer structure and it is assumed that the thickness of the layer is uniform. The saturation magnetization of the core area is considered to be ${M_s}^{core}$ and that of the layer area is ${M_s}^{layer}$. Both ${M_s}^{core}$ and ${M_s}^{layer}$ contribute to the total M_s of the rod by their volume fraction. M_s can be calculated from

$$M_s = \frac{V_{core}{M_s}^{core} + V_{layer}{M_s}^{layer}}{V}, \tag{3.6}$$

where V_{core} is the volume of the core and V_{layer} is the volume of the layer. Let r be the radius of the rod and d be the case depth, then

$$M_s = \frac{(r-d)^2}{r^2}{M_s}^{core} + \frac{[r^2-(r-d)^2]}{r^2}{M_s}^{layer}, \tag{3.7}$$

and finally M_s can be expressed as a second order polynomial of d

$$M_s = (1 - \frac{2d}{r} + \frac{d^2}{r^2}){M_s}^{core} + (\frac{2d}{r} - \frac{d^2}{r^2}){M_s}^{layer}. \tag{3.8}$$

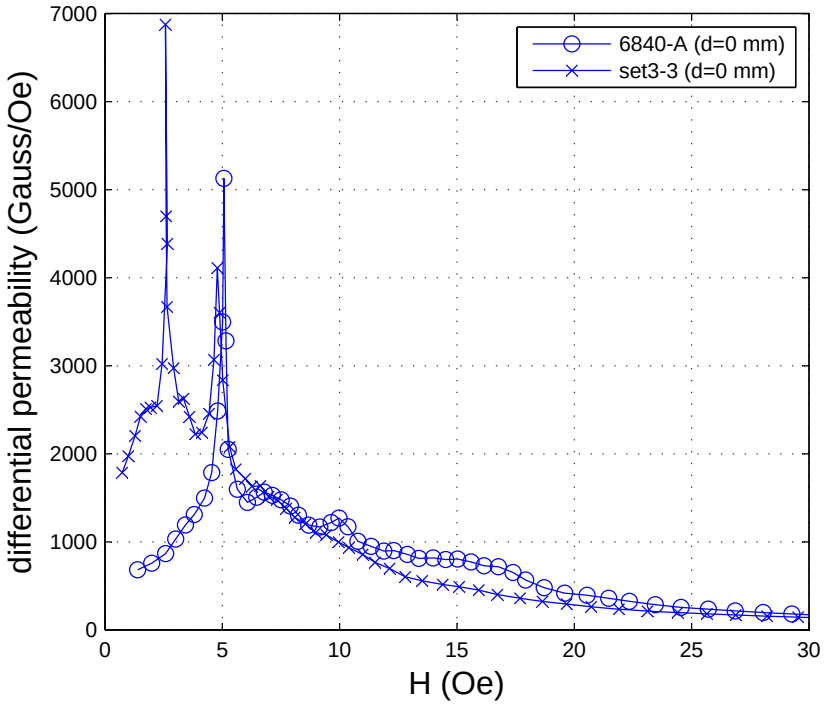

Figure 3.9 Differential permeability versus applied magnetic field for 1" 8620 steel rods with no surface hardening. Set3-2 is 'as received' and 6840-A was heat treated but not surface hardened.

3.4.3 Experiment

Hysteresis loop measurements were completed on the induction hardened and carburized 1" diameter and 17.5" long steel rods. Magnetic field in the range of -1200 Oe to 1200 Oe was supplied by the LDJ 3600 series from LDJ Electronic, Troy, MI. The measurement was controlled by the LDJ 3600 software. A pick-up coil with 372 turns, which encircles the middle part of the plastic holder for the sample, was used to measure the induction B. The output of the measurements is composed of the value of applied magnetic field and that of the magnetic induction.

By observing the B-H plot of the samples, B saturates when H is around 300 Oe. The value of H between 800 Oe and 1200 Oe was used to find M_s. M can be calculated from

$$M = \frac{B - H}{4\pi}, \tag{3.9}$$

Then M is plotted versus $1/H^2$. A second order polynomial is fitted to the data points and the M intercept is the value of M_s using

$$M = M_s \left(1 - \frac{b}{H^2}\right). \tag{3.10}$$

The M_s found by adding a second order polynomial to the measured data of sample 7396 is show in Figure 3.10. M is plotted as a function of $1/H^2$ and M_s of this sample equals to 1756.12 emu/cm^3.

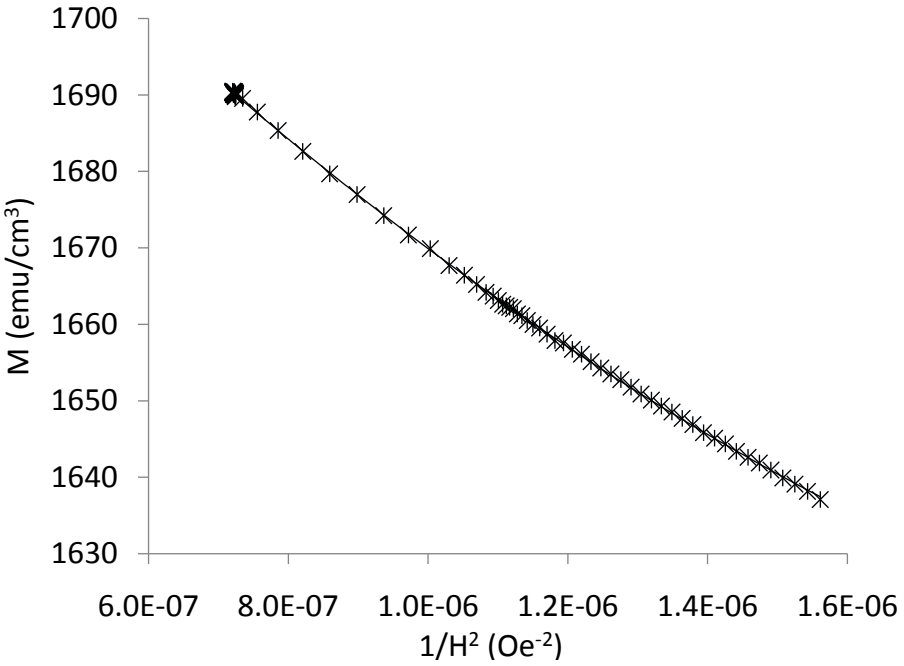

Figure 3.10 Saturation magnetization obtained by fitting a second order polynominal to the measured data of sample 7396. M_s=1756.12 emu/cm^3.

3.4.4 Sources of error or uncertainty

The first results we got show the trend that the saturation magnetization M_s gets smaller as the case depth increases, which is as expected. However, the experimental maximum value of M_s is about 10 percent bigger that the M_s of pure iron at room temperature. One of the possible reasons for this is that the applied current is not big enough to reach a good saturation state. We increased the working current to twice of the original value to solve this problem, and

the M_s decreased by about 2 percent, so it can be concluded that this is not the main source of error. Second, the measured H may be not be the same as the magnetic field inside the sample. In order to make the measurement more accurate, we measured the applied magnetic field H_{app} instead, and calculated M using

$$B = 4\pi M + H_{in}, \tag{3.11}$$

$$H_{in} = H_{app} - N_d M, \tag{3.12}$$

$$M = \frac{B - H_{app}}{4\pi - N_d}, \tag{3.13}$$

where N_d is the demagnetizing factor. N_d is equal to 0.00617 for cylinder with $l/d = 20$. Another possible source of error or uncertainty is the pick up coil which encircles the outside of the plastic holder. The pick up coils measures both the flux inside the sample and the flux in the area between the outside of the sample and the pick-up coil. The induction B was calculated using

$$B = \frac{\Phi}{A}, \tag{3.14}$$

where Φ is the flux measured by the pick up coil and A is the cross section area of the sample. The calculated B is bigger than its real value because the flux in the area between the sample and the pick-coil is also included in the calculation. In order to corrected this, an equation is calculated based on the outer diameter of the pick-up coil and the diameter of the sample. $B_{corrected}$ is got from

$$B_{corrected} = B_{measured} - \frac{H({r_{coil}}^2 - {r_{rod}}^2)}{{r_{rod}}^2}, \tag{3.15}$$

then M can be interpreted from

$$M = \frac{B_{measured} - \frac{H({r_{coil}}^2 - {r_{rod}}^2)}{{r_{rod}}^2} - H}{4\pi}, \tag{3.16}$$

$$B_{measured} = \frac{\Phi_{measured}}{\pi {r_{rod}}^2}, \tag{3.17}$$

$$M = \frac{\frac{\Phi_{measured}}{\pi {r_{rod}}^2} - \frac{H({r_{coil}}^2 - {r_{rod}}^2)}{{r_{rod}}^2} - H}{4\pi}. \tag{3.18}$$

The magnetization M is determined from four quantities r_{coil}, r_{rod}, $B_{measured}$ and H through equation 3.16. The combined standard uncertainty of the measurement result $u(M)$, may be determined from [17]

$$u(M)^2 = \left(\frac{\partial M}{\partial r_{coil}}\right)^2 u^2(r_{coil}) + \left(\frac{\partial M}{\partial r_{rod}}\right)^2 u^2(r_{rod}) + \left(\frac{\partial M}{\partial B_{measured}}\right)^2 u^2(B_{measured}) + \left(\frac{\partial M}{\partial H}\right)^2 u^2(H), \tag{3.19}$$

commonly referred to as the law of propagation of uncertainty. $u(x)$ is the standard uncertainty associated with x. It can be calculated from equation 3.16 that

$$\frac{\partial M}{\partial r_{coil}} = -\frac{H r_{coil}}{2\pi {r_{rod}}^2}, \tag{3.20}$$

$$\frac{\partial M}{\partial r_{rod}} = -\frac{B_{measured}}{2\pi r_{rod}} + \frac{H {r_{coil}}^2}{2\pi {r_{rod}}^3}, \tag{3.21}$$

$$\frac{\partial M}{\partial B_{measured}} = \frac{1}{4\pi}, \tag{3.22}$$

$$\frac{\partial M}{\partial H} = -\frac{1}{4\pi} - \frac{H({r_{coil}}^2 - {r_{rod}}^2)}{4\pi {r_{rod}}^2}. \tag{3.23}$$

The standard uncertainty associated with M when H is equal to 1100 Oe was calculated and shown in Table 3.2 for the induction-hardened steel rods and in Table 3.3 for the carburized steel rods.

Table 3.2 The standard uncertainty associated with M when H is equal to 1100 Oe for the induction-hardened steel rods.

Sample	Profile depth with uncertainty due to the rotation of rod(mm)	M (emu/cm^3)	u(M) (emu/cm^3)
7396	3.30 ± 0.02	1683	47
7395	2.27 ± 0.04	1702	47
7394	1.43 ± 0.02	1715	47
7393	0.90 ± 0.04	1742	45
7397	0	1762	45

3.4.5 Results

The M_s values of the induction-hardened steel rods are given in Table 3.4 while those of the carburized steel rods are given in Table 3.5. The ${M_s}^{core}$ of the surface-hardened steel rods is the value of M_s when the case depth is 0, which is provided by sample 7397 for the induction-hardened rods and sample 6840 for the carburized rods. ${M_s}^{layer}$ can be calculated

Table 3.3 The standard uncertainty associated with M when H is equal to 1100 Oe for the carburized steel rods.

Sample	Profile depth with uncertainty due to the rotation of rod(mm)	M (emu/cm^3)	u(M) (emu/cm^3)
6807	1.58 ± 0.02	1720	47
6805	0.97 ± 0.01	1737	45
6804	0.80 ± 0.02	1766	49
6803	0.54 ± 0.02	1779	45
6840	0	1833	44

using equation 3.7 for each sample and the results were averaged. After putting the value of average radius r, ${M_s}^{core}$ and average ${M_s}^{layer}$ into equation 3.7, the relationship between the total M_s of induction-hardened steel rods and case depth d is

$$M_s = 0.89d^2 - 22.50d + 1821.38. \tag{3.24}$$

For the carburized steel rods,

$$M_s = 2.8624d^2 - 71.2739d + 1871.38. \tag{3.25}$$

Magnetization of the induction hardened steel rods plotted as a function of case depth is shown in Figure 3.11, while M_s of the carburized samples plotted versus case depth is shown in Figure 3.12. The curve representing the relationship between M_s and d calculated from the model was added to the experimental data to make a comparison. For both induction-hardened and carburized steel rods, M_s decreases as the case depth increases and there is good agreement between the model and the experimental data.

Table 3.4 Saturation magnetization of induction hardened steel rods with calculated uncertainties.

Sample	Profile depth with uncertainty due to the rotation of rod(mm)	M_s (emu/cm^3)	u(M_s) (emu/cm^3)
7396	3.30 ± 0.02	1756	49
7395	2.27 ± 0.04	1774	49
7394	1.43 ± 0.02	1789	47
7393	0.90 ± 0.04	1805	47
7397	0	1821	46

Table 3.5 Saturation magnetization of carburized steel rods with calculated uncertainties.

Sample	Profile depth with uncertainty due to the rotation of rod(mm)	M_s (emu/cm^3)	u(M_s) (emu/cm^3)
6807	1.58 ± 0.02	1774	48
6805	0.97 ± 0.01	1780	47
6804	0.80 ± 0.02	1820	51
6803	0.54 ± 0.02	1831	46
6840	0	1871	46

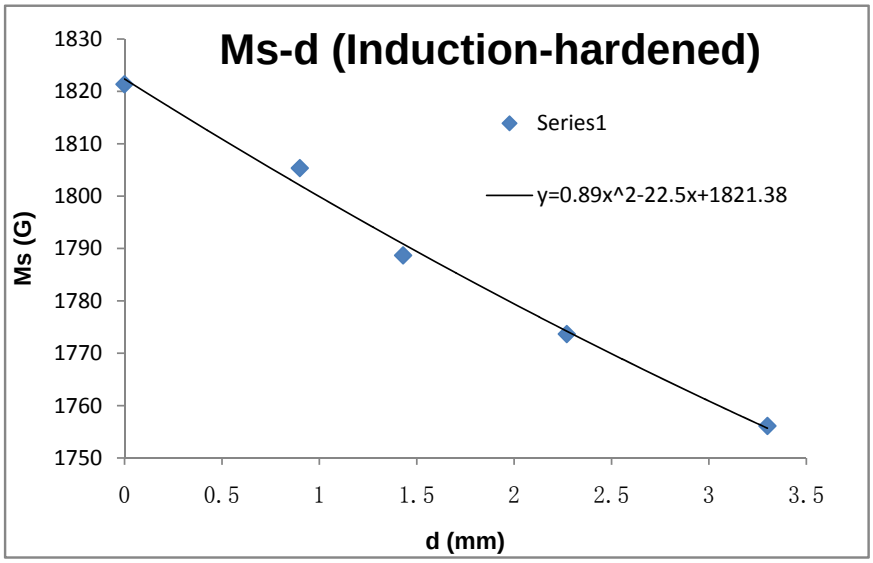

Figure 3.11 Saturation magnetization (M_s) plotted as a function of case depth (d) of induction-hardened steel rods. A curve representing the relationship between M_s and d calculated from equation 3.24 is added to the experimental data for comparison.

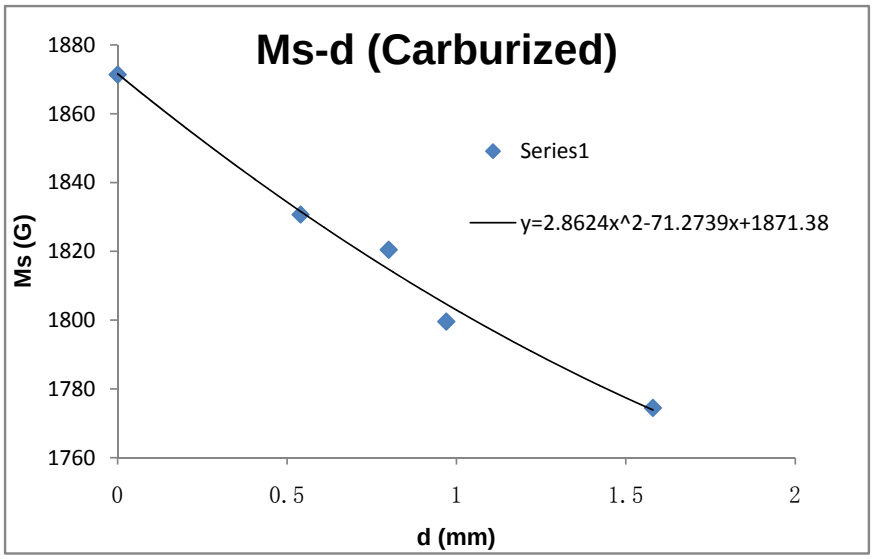

Figure 3.12 Saturation magnetization (M_s) plotted as a function of case depth (d) of carburized steel rods. A curve representing the relationship between M_s and d calculated from equation 3.25 is added to the experimental data for comparison.

CHAPTER 4. ALTERNATING CURRENT POTENTIAL DROP MEASUREMENTS ON CASE HARDENED STEEL RODS

The surface hardening process is used to improve the wear resistance of steel parts. Case depth is essential for the quality control in the process. The electrical conductivity (or resistivity) and magnetic permeability of the surface steel are modified by the hardening process. Four-point potential drop methods can be used to determine material properties nondestructively, such as conductivity and permeability.

It was shown that case depth can be evaluated nondestructively by measuring resistivity using four point probes method, which is based on the calibration curve established previously for the same material [9]. Potential drops measured with two sensors that differ in the probe spacing were used to evaluate case depth on the surface of induction hardened steel.

In this chapter, four-point ACPD measurements made on surface hardened steel rods are described with the aim of finding a way to evaluate the case depth.

4.1 Introduction

In ACPD measurements, the current is generally injected into the specimen by direct contact. When the current passes through the sample, it can only flow in a thin layer on the outer surface due to the so called "skin effect". The depth of the current carrying layer, usually referred to "skin depth", δ, is given by

$$\delta = \frac{1}{\sqrt{\pi \sigma \mu_r \mu_0 f}} \tag{4.1}$$

Where σ is the electrical conductivity of the conductor, μ_r is its relative magnetic permeability, μ_0 is the permeability of free space, and f is the frequency of the applied alternating current.

Materials of high permeability or conductivity thus have relatively small skin depths. At a frequency of about 5 kHz, for example, ferromagnetic mild steel has a skin depth of order 0.1 mm, high conductivity materials such as aluminium and zinc have skin depths of 1–2 mm, and low conductivity metals such as titanium and stainless steel have skin depths of 5–8 mm.

For a certain material, the skin depth varies with the frequency of the alternating current applied, causing changes in the potential drop measured. When applied to case hardened steel, ACPD has the potential to estimate the case depth. At low frequency when the skin depth is bigger than the case depth, the measured potential drop is determined by both the case and inner layer properties. When the frequency is so high that the penetration depth is smaller than the case depth, the potential drop is mainly determined by the surface layer properties. Thus material properties can be evaluated by making multi-frequency ACPD measurements.

4.2 Review of potential drop methods for material property measurements

The electric potential drop method has been recognized as a reliable, economic and precise crack measurement technique. However, its application includes not only defect detection and sizing but also material identification and determination of different geometrical and material properties [18]. In a four-point alternating current potential drop (ACPD) measurement, there are two current electrodes and two voltage electrodes. Alternating current is injected into the surface of a conductor and the potential drop is measured between the voltage electrodes (Figure 4.1). Another four-point potential drop method is direct current potential drop (DCPD) method, in which direct current instead of alternating current passes through the current electrodes.

Four-point probe method is another widely used technique for measurement of the resistivity of a semiconductor or conductor. It uses DC current and has been applied on rectangular solids, circular disks and cylindrical materials [19], [20], [21], [22].

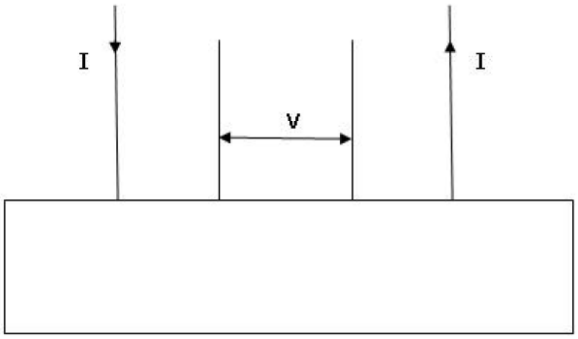

Figure 4.1 Arrangement of a four-point potential drop system. Alternating current is applied to the sample via the outer pair of current electrodes. The potential drop is measured between the inner pair of voltage electrodes.

4.2.1 Plate geometry

Multi-frequency four point alternating current potential drop (ACPD) measurements can be used to determine the parameters of conductive plates such as electrical conductivity, magnetic permeability and plate thickness non-destructively [17]. The measured pick up voltage is matched with voltage measurements. Results are calculated from an analytical expression in which the potential drop is expressed in terms of parameters describing the sample and probe. A theoretical model is needed to get the values of these parameters from the measured potential drop. In reference [23] ACPD voltage values were developed as series solutions and compared with experimental data taken on a titanium plate. The plate thickness is approximately two-thirds of the probe length. Generally, the ACPD measured between the two pickup points of a four-point probe in contact with a conductive surface was written as

$$V = \frac{I}{2\pi\sigma}\left[F_k(\rho_{22}) - F_k(\rho_{21}) - F_k(\rho_{12}) + F_k(\rho_{11})\right], \tag{4.2}$$

where V is the complex voltage, I is the amplitude of the current injected and σ is the conductivity. $F_k(\rho)$ can take different forms for half-space conductors, thick plates and thin plates. Thick plates refer to plates that are somewhat thicker than the probe dimensions and thin plates refer to plates that are somewhat thinner.

In the case of a half-space conductor

$$F_{hs}(\rho) = \frac{e^{ik\rho}}{\rho} + ik\left[E_1(-ik\rho) + \left(1 - \frac{ikh}{\mu_r}\right)\ln\rho\right] \tag{4.3}$$

This result agrees with equation (31) in reference [24]. In (2) $\mu_r = \mu/\mu_0$ is the relative permeability of the half-space. Two forms of $F_k(\rho)$ in the case of plates were given

$$\begin{aligned} F_p(\rho) &= -ik\left[\coth\left(\frac{ikc}{2}\right) + \frac{ikh}{\mu_r}\right]\ln\rho \\ &\quad + \sum_n \left(\frac{\exp\left[ik\sqrt{\rho^2 + (nc)^2}\right]}{\sqrt{\rho^2 + (nc)^2}} + ike^{iknc}E_1\left\{-ik\left[\sqrt{\rho^2 + (nc)^2} - nc\right]\right\}\right) \end{aligned}$$

The above equation converges more rapidly for thick plates. $c/2$ is the plate thickness, h is the height of the measurement circuit. $k^2 = i\omega\mu\sigma$, where m is the magnetic permeability and s is the electrical conductivity of the material.

$$\begin{aligned} F_p(\rho) &= -ik\left[\coth\left(\frac{ikc}{2}\right) + \frac{ikh}{\mu_r}\right]\ln\rho \\ &\quad + \frac{4}{c}\sum_{\upsilon=1}^{\infty} \frac{(2\pi\upsilon)^2}{(2\pi\upsilon)^2 - (kc)^2} K_0\left[(\rho/c)\sqrt{(2\pi\upsilon)^2 - (kc)^2}\right] \end{aligned}$$

The above equation converges more rapidly for thin plates.

Finally, an approximation for plates somewhat thinner than the probe point separations was given

$$F_{tp} \approx -ik\left[\coth\left(\frac{ikc}{2}\right) + \frac{ikh}{\mu_r}\right]\ln\rho, c/\rho \ll 1, \tag{4.4}$$

The above equation agrees with equation (9) in reference [17].

In reference [17] ACPD method is used to determine the conductivity, relative permeability and thickness of homogeneous metal plates. The frequency range used was from 1 Hz to 10 kHz.These parameters can be calculated using the analytical expressions developed. For a symmetric, linear probe

$$V = \frac{I}{\pi}\left[-\frac{ik}{\sigma}\coth(ikT) + i\omega\mu_0 I\right]\ln\left|\frac{1+a}{1-a}\right| \tag{4.5}$$

Where T is the thickness of the plate and a is the ratio of the position of the pickup point to the position of the source point. An analytical expression for the electric field in a half space

conductor, due to alternating current injected at the surface was derived in reference [25]. In the conductor, the total electric field $\mathbf{E}^T$ was given by

$$\mathbf{E}^T(\mathbf{r}) = \mathbf{E}(\mathbf{r}_+) - \mathbf{E}(\mathbf{r}_-) \tag{4.6}$$

Alternating current was injected and extracted by contact wires at $x = \pm S$.

$$r_\pm = \sqrt{(x \pm S)^2 + y^2 + z^2} \tag{4.7}$$

The components of $\mathbf{E}$ were given by

$$E_z(\mathbf{r}) = -\frac{i\omega\mu I}{2\pi}\frac{ikz}{(ikr)^3}e^{ikr}(1 - ikr), z > 0. \tag{4.8}$$

$$E_\rho(\mathbf{r}) = \frac{i\omega\mu I}{2\pi}\frac{1}{ik\rho}\left\{e^{ikz} - \frac{e^{ikr}}{ikr}\left[1 + \frac{(ikz)^2}{ikr}\left(1 - \frac{1}{ikr}\right)\right]\right\} \tag{4.9}$$

The main source of uncertainty in the four-point conductivity measurement is scatter in the voltage measurements. The uncertainty in the ACPD technique is smaller than that in eddy current measurements [26]. The four point ACPD method is also easy to use without the need for calibrating specimens. Moreover, the four-point approach is independent of magnetic permeability below a certain characteristic frequency and can be used to measure conductivity of ferrous metals such as steel.

4.2.2 Cylindrical geometry

The suitable arrangement of probes to measure case depth of materials with cylindrical geometry by using four-point DCPD was considered in reference [9]. A surface hardened shaft like material is modeled as a two layer structure which has two different conductivity σ_1 (resistivity ρ_1) at surface hardened part and σ_0 (resistivity ρ_0) at inner untreated part as shown in Figure 4.2, where d is the case depth of shaft.

Two kinds of arrangements of probes were examined. One is the arrangement in the axial direction and the other is in the circumferential direction (Figure 4.3). For the former arrangement, the lengths of four probes are always equal to each other and the sensor for measurement on a flat plane can be used for any cylindrical parts with different diameter. By locating the

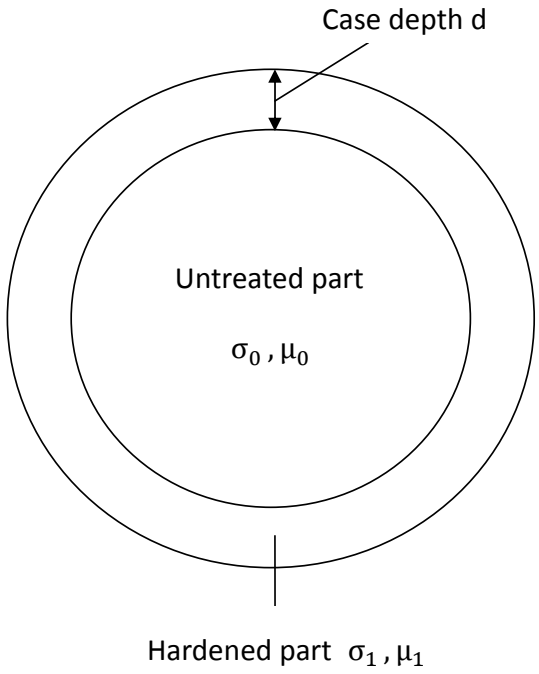

Figure 4.2 Model of surface hardened shaft like material

probes in circumferential direction, high density current may flow across the boundary between the case and the core as shown in Figure 4.3. Thus improvement of sensitivity to evaluate case depth can be expected. Different sensors would be needed for materials with different diameter because the lengths of four probes change with diameter.

The results show that in both cases the potential drop V increases with the case depth d, but the increasing rate of V decreases. The distance of two probes for current input and output should be taken larger to evaluate deeper case depth. The measurement probes should be located near the current input-output probes to evaluate smaller case depth sensitively.

In order to examine the change in resistivity with hardening, steel specimens were quenched under several conditions. Then the resistivity and hardness were measured. The resistivity of the specimen ρ can be calculated from the following equation [9]:

$$\rho = \frac{\pi}{2I} \frac{(S_1^2 - S_2^2)}{S_2} \frac{V}{k} \tag{4.10}$$

The potential drop V was measured by the measuring probes. $2S_1$ is the distance of two probes

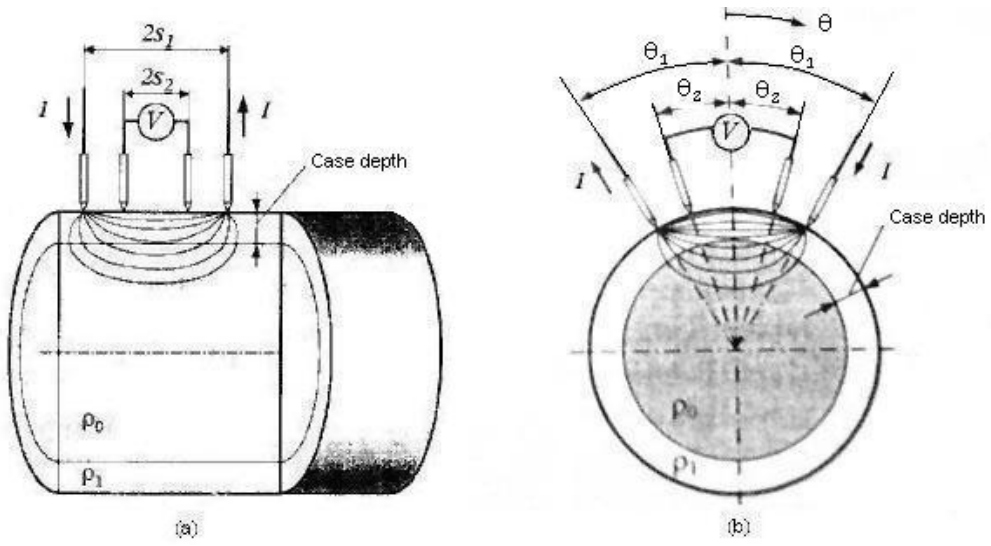

Figure 4.3 Two ways of arranging the probe: (a) Probe in an axial direction. (b) Probe in a circumferential direction. (Source: [9])

for current input and output, $2S_2$ is the distance of two probes for measuring potential drop. Measured potential drop V is affected by the size and shape of the specimen. Coefficient k is the shape correction factor, which is unity in the case of semi-infinite material. The value of k was obtained by using finite element method (FEM). The result confirmed that resistivity, which can be measured using four-point probe method, increases with hardening.

The case depth of induction-hardened steel rods was determined using two-point ACPD method in [27]. The steel rod is assumed to be a two-layer structure which is uniform in the axial direction as shown in Figure 4.2. The theory of the electromagnetic field in a homogeneous rod was described first, then a generalized ACPD theory was developed for a layered rod. An axially-symmetric alternating electrical current is passed down a rod and ACPD measurements were made on the induction-hardened rod in the range of frequencies for 1 Hz to 10 kHz. The electrical conductivity, permeability and case depth of the outer layer were adjusted to find an optimum least squares fit of ACPD model predictions. The case depths found in this way exceed those obtained from hardness measurement at 50 HRC by about 30% and sources of error were discussed. The measurement system used in reference [27] is not practical for case depth measurement in industry. However, the results suggest that a model-based approach

using multi-frequency four-point ACPD could satisfy the industrial need for nondestructive evaluation of case depth.

4.2.3 Delicate materials

The conventional four-point probe method is suitable for system where the conductivity is homogeneous comparing to the electrode spacing. The atomic force microscopic (AFM) probe is now being applied as a four-point probe to measure the superficial or local conductivities for delicate materials. In reference [28], a four-point AFM probe with a minimized electrode spacing as small as 1.0 μm was demonstrated.

The electrical potential drop V was derived from

$$V = \rho \frac{I}{2\pi} \left[\frac{1}{S_1} + \frac{1}{S_3} - \frac{1}{(S_1 + S_2)} - \frac{1}{(S_2 + S_3)} \right] \tag{4.11}$$

Which means

$$\rho = \frac{2\pi(V/I)}{\left[\frac{1}{S_1} + \frac{1}{S_3} - \frac{1}{(S_1+S_2)} - \frac{1}{(S_2+S_3)} \right]} \tag{4.12}$$

The above two equations agree with equation (1.7) and (1.8) in reference [29], where the four-point probe technique was used to measure the semiconductor resistivity. These are essentially the basic expressions for four point DCPD on a flat surface of half space conductors. S_2 is the distance between the voltage electrodes, S_1 and S_3 are the distances between the current electrodes to the nearest voltage electrodes. The mechanical contact between the probe and the surface is enough to obtain reliable electrical contact to samples. The minimized electrode spacing allows current to flow very close to the surface during topography scanning. The four-point AFM probe is capable of measuring the local conductivity of fragile objects, biomaterial surfaces and thin films on a scale of several microns.

4.3 Experiment

The steel rods were demagnetized before the ACPD measurements. A rod was put into a plastic holder which was put into inside a 48-cm long solenoid with diameter 9-cm. The current flowing in the solenoid was provided by a Kepco bipolar operational power supply/amplifier,

model number BOP 50-8M. The current was reduced from a value high enough to nearly saturate the samples (8 A) to zero through a period of 62 cycles, which took about 48 seconds. It was checked using a gaussmeter that the residual magnetic induction of the samples is smaller than 3 gauss.

ACPD measurements were made as a function of frequency on the induction hardened 4140 steel rods and carburized 8620 steel rods with the diameter of 1". The range of frequency is from 1 Hz to 10 kHz. Electrical contact with the steel rods was made using four GSS-8-7-G probes from Interconnect Devices Inc. (IDI), which were held perpendicular to the surface of the steel rod. The four contact points were arranged in a straight line parallel to the axis of the rod. There is a common midpoint between the two current drive points and two pick-up points. The distance between the current injection and extraction points of the co-linear four-point probe used in these measurements is 74.2 mm. The distance between the symmetrically-placed voltage pick-up points is 24.7 mm.

The rod was put on a simple plastic holder that was designed and made for the ACPD measurements on rods with 1" diameter. The four pins are held at the bottom of the bottom plastic block, which is attached to the bottom of a bigger top plastic block. The top plastic block is fixed on the holder using plastic screws in such a way that the pins contact the rod directly and the four probes points are placed parallel to the rod axis. The wires pass through the bottom plastic block and the top plastic block (Figure 4.4).

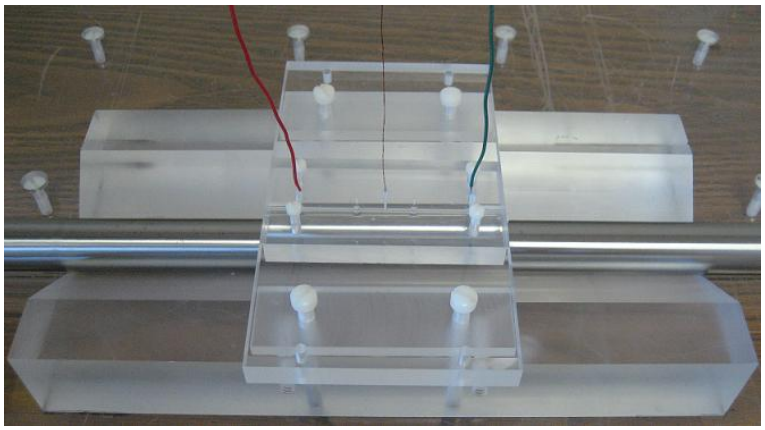

Figure 4.4 Four point ACPD measurement of surface hardened steel rods

The two current wires were held perpendicular to the rod surface for a distance of about 30 cm above the rod and then twisted together to reduce interwire capacitance. In order to minimize the inductance in the measurement circuit, the two voltage pick-up wires ran along the underside of the plastic block holding the pick-up contacts and lay as close to the surface of the sample as possible. They were twisted together at the midpoint between the pick-up points.

The alternating current was injected into the steel rod through the current wires by a Kepco BOP 36-12M power supply. The sine signal from the internal function generator of a Stanford Research Systems SR830 DSP lock-in amplifier was connected to the current programming input of the power supply, with the power supply working as a current drive.

A high precision resistor was connected in series with the drive current circuit in order to monitor the current and the voltage across the resistor was measured. The resistance maintains one percent accuracy over the range of frequency for which it could be measured with an Agilent 4294A precision impedance analyzer; 40 Hz to 40 kHz. The voltage across the resistor and that of the pick-up probe were both measured using the SR830 lock-in amplifier. In order to make both voltage measurements using the same lock-in amplifier, a switch was used activated by a control signal from the auxiliary analog output of the lock-in amplifier.

It is necessary to correct the experimental data for common-mode rejection (CMR) error in the lock-in amplifier [30]. This systematic error shows itself by the fact that, when the pick-up terminals are reversed, the measured voltage changes by a few μV. The magnitude of the error is, therefore, similar to that of the voltage being measured, and a corrective procedure is essential. The CMR error was eliminated by taking two sets of measurements, reversing the pick-up terminals for the second. The two sets were then subtracted and the result divided by two.

The ACPD measurements were controlled automatically by a computer program developed before [30]. The lock-in amplifier was connected to the computer using a GPIB bus. The control program sends commands to the lock-in amplifier to set all the measurement parameters, and then the measured data are sent back to the control program. A detailed discussion of the

program was given in reference [30].

4.4 Results

The measured real and imaginary impedance of the un-hardened rod 7397 were plotted as a function of frequency and the results are shown in Figure 4.5. In the low-frequency range of the ACPD measurement, the measured voltage is independent of magnetic permeability [17]. Initially, the real impedance (R) tends to a constant value (DC value) and the imaginary part (L) is approximately zero. Then R increases approximately linearly with frequency f from its DC value which is independent of permeability as shown in equation (9) of reference [27], the expression for the low frequency impedance limit is

$$R \approx \frac{1}{\pi a^2 \sigma}\left(1 + \frac{a^2}{48\delta^2} + \ldots\right) \tag{4.13}$$

and

$$L \approx \frac{\mu}{8\pi}\left(1 + \frac{a^2}{96\delta^2} + \ldots\right), \tag{4.14}$$

where a is the radius of the rod and δ is the skin depth that equals to $1/\sqrt{\pi f \sigma}$. The leading term for L in equation (9) of reference [27] is proportional to permeability and independent of conductivity. Thus it is possible to determine both the conductivity and permeability of the rod from R and L at low frequency.

Real and imaginary parts of the measured impedance were normalized (The normalized real impedance $R_{normalized}$ of a surface-hardened rod is equal to $R_{hardend}$ of that sample divided by $R_{unhardened}$ of the unhardened rod, the normalized imaginary L was obtained in the same way.) with respect to data taken on heated but not hardened samples and plotted as a function of frequency. Results for the induction-hardened rods are shown in Figure 4.6, and those for the carburized rods in Figure 4.7. At low frequencies the real part of the normalized impedance indicates the overall resistance of the rod, which is bigger than that of the untreated rod as a result of the case hardening. The normalized real impedance increases with the case depth at low frequencies when the skin depth is bigger than diameter of the rod, which agrees with the low-frequency part of Figure 8 in reference [27]. The imaginary part of the data is noisy at

low frequencies because the signal is tending to a purely resistive (real) component, with zero imaginary part, as the frequency tends to zero. The little peak in the plot of the normalized imaginary impedance for the induction-hardened rods may be caused by a measured value that is smaller than the real value of L for the baseline sample. Generally, the overall permeability decreases with case depth, as shown by the decrease in the imaginary part of the normalized impedance at low frequency.

The normalized real impedance when the frequency is 1 Hz is plotted as a function of mid-hardness depth for both induction-hardened and carburized steel rods in Figure 4.8. A linear fit to each data set is also shown. It can be seen that the fitted line tends to a normalized real impedance of one when the case depth is zero (for unhardened rod) in both cases, as expected. There is less scatter about the linear fit to the data for the induction-hardened rods than for the carburized samples. However, even in the case of carburized rods, this technique is promising for evaluating depth of case hardening from four-point potential drop measurements.

It was shown that the four-point potential drop measurement is a promising technique for nondestructive evaluation of case depth. The relationship between the measured impedance Z and case depth d in the low frequency range will be studied in more details based on the four-point DC theory in the next period. Model-based data-fitting will be performed to estimate the depth of case-hardening from these measurements. In addition, modeling of the AC field would make use of the whole set of data instead of just the low frequency part, and might improve the accuracy of measured case depth. The principle of this technique has been demonstrated earlier by a two-point ACPD measurement on induction hardened steel rods in reference [27], in which axially symmetric alternating current was applied. In a manufacturing environment, four-point potential drop measurement is needed to monitor case hardened steel components. That is because it is not practical to apply an axially-symmetric current on small components. Also, applying an axially-symmetric current is not feasible for rapid inspections when taking measurements on large numbers of rods

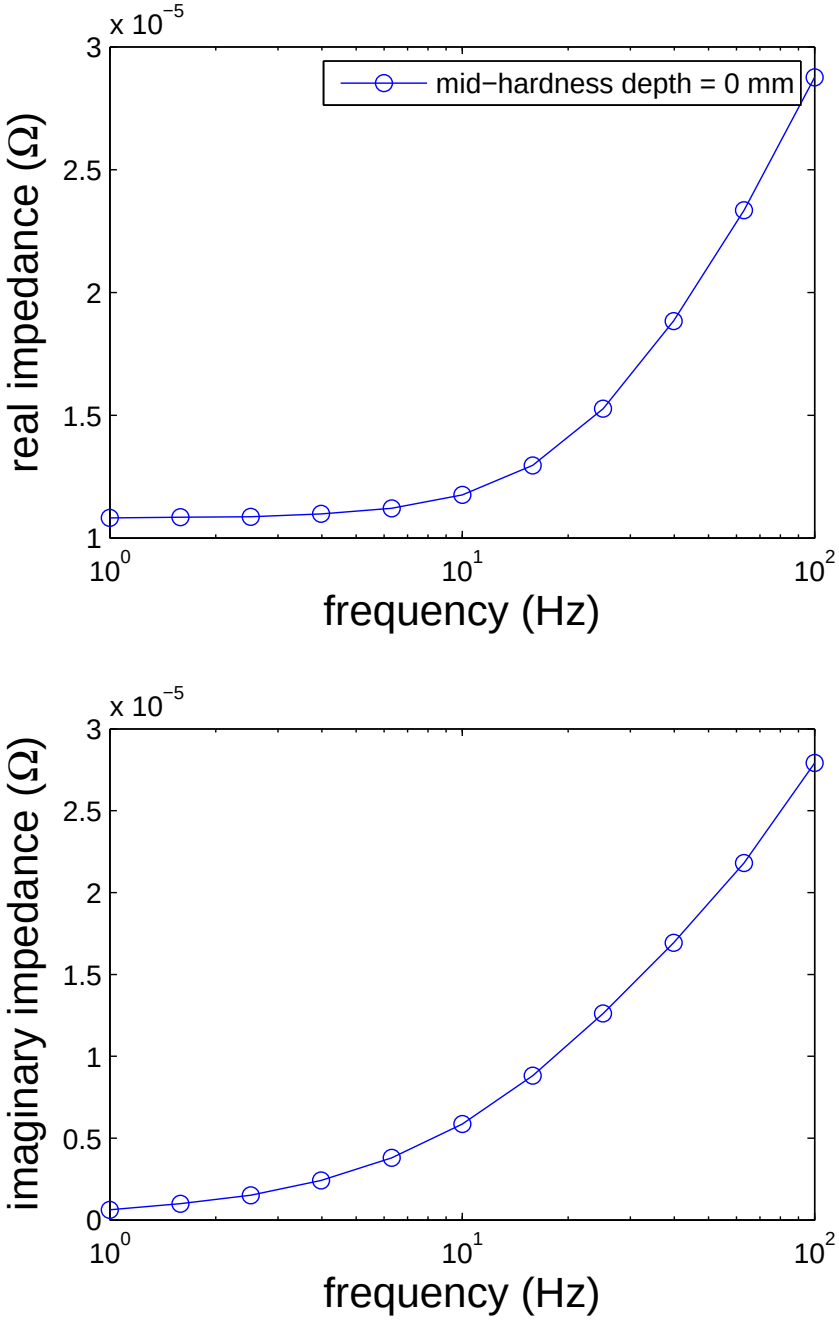

Figure 4.5 Real and imaginary parts of the measured impedance of an unhardened rod as a function of frequency derived from ACPD data.

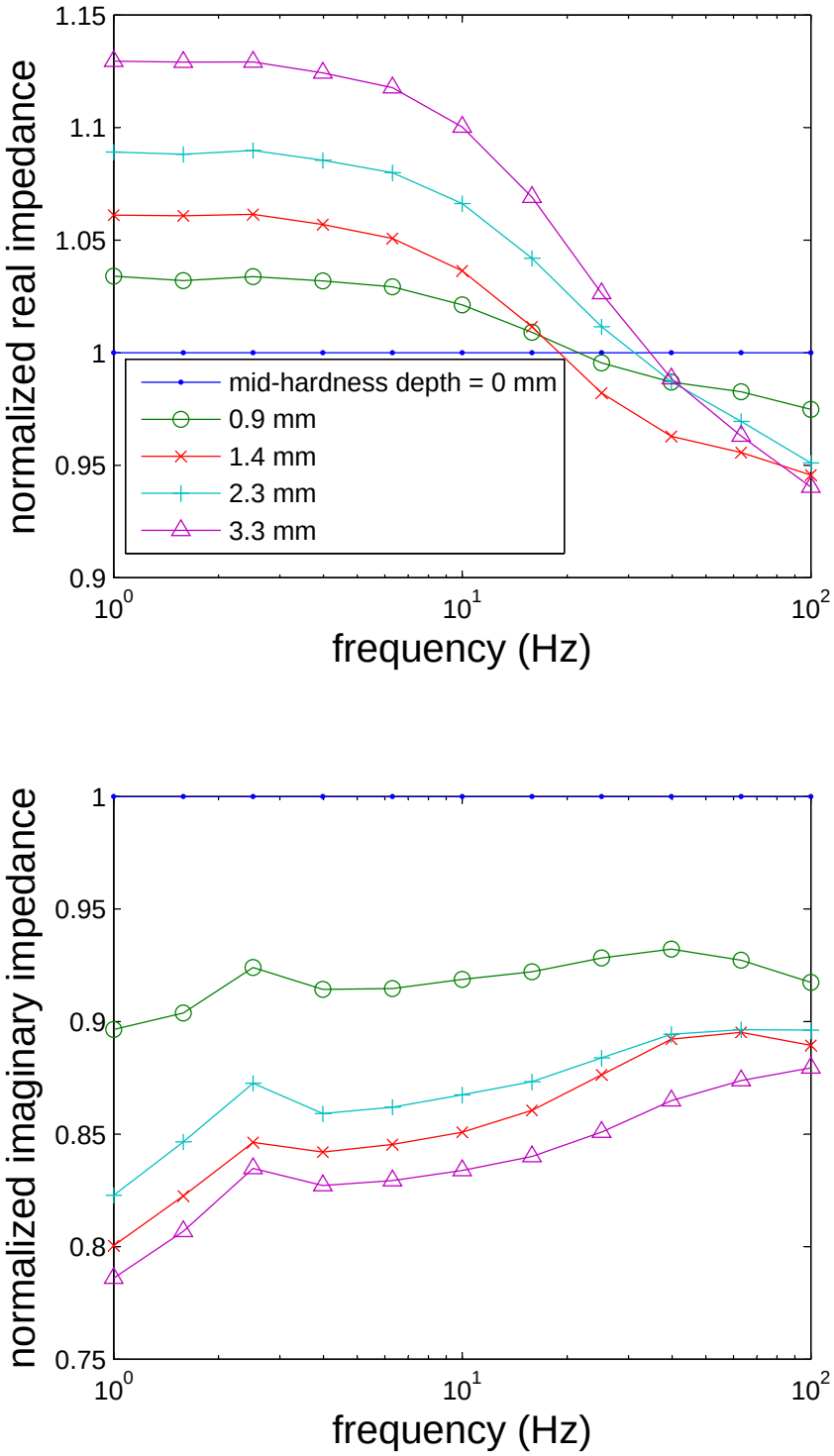

Figure 4.6 Real and imaginary parts of the normalized impedance as a function of frequency derived from ACPD data on induction hardened rods of 1" diameter.

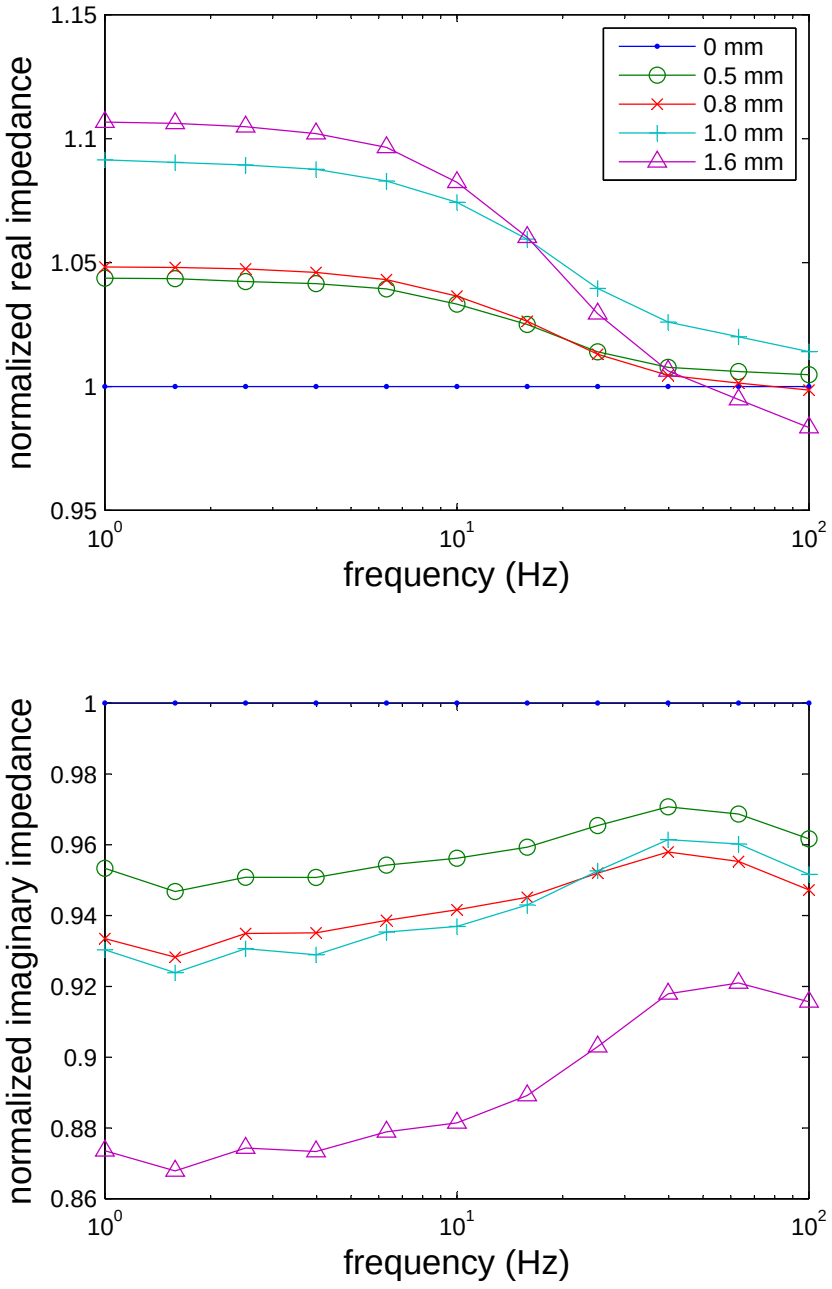

Figure 4.7 Real and imaginary parts of the normalized impedance as a function of frequency derived from ACPD data on carburized rods of 1" diameter.

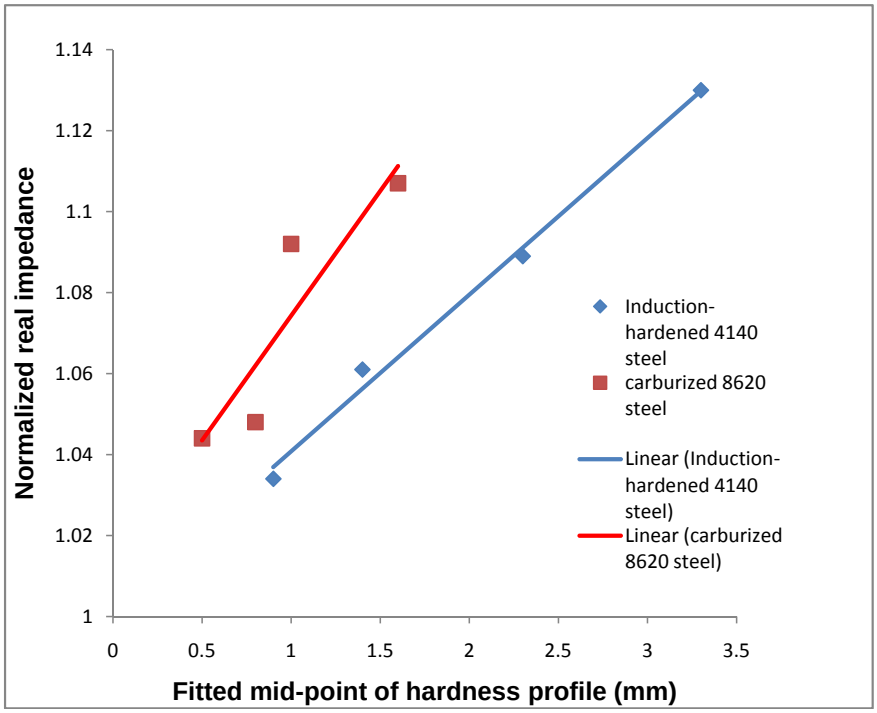

Figure 4.8 Value of the normalized real impedance when the frequency is 1 Hz versus mid-hardness depth for both induction-hardened and carburized steel rods. A linear fit to each data set is also shown.

CHAPTER 5. CONCLUSION AND FUTURE WORK

5.1 Summary

The magnetic properties of a series of surface-hardened steel rods, including initial permeability, differential permeability and saturation magnetization were studied with the aim of evaluating the depth of case hardening nondestructively. Four-point alternating potential drop measurements were also made on the induction-hardened 4140 and carburized 8620 steel 1" diameter rods using a co-linear probe with pins aligned in a line parallel to the axis of the rod.

Case depth of the surface-hardened steel rods were first determined from the hardness profiles completed on both induction-hardened and carburized samples, in order to compare with the electromagnetic measurements.

It was shown that differential permeability measurements give a good indication of case depth in induction hardened rods, but not carburized rods. The saturation magnetization decreases as a second order polynomial when the case depth increases. By measuring the change in resistivity caused by case hardening, different depth of case hardening can be determined using the four-point ACPD technique, especially in the low-frequency range. By observing the real part of the normalized impedance, there is good distinction between the case depths of the samples.

5.2 Future research

The four-point ACPD measurement is a promising technique to determine the case depths of the rod samples. The principle has been demonstrated before via a two-point ACPD measurement [27] in which the current is homogeneous between the pick-up points so that the electric field varies only in one dimension and the model is simple. Four-point ACPD is needed

because it is inconvenient to inject an an axially-symmetric current when taking measurements on large numbers of rods, and it is not feasible when the dimension of rod is too small [31]. Model-based data fitting would need to be performed to estimate the case depth from four-point ACPD measurements on these samples. The accuracy of the four-point DCPD technique will be assessed first by applying a DC model to the low-frequency part of the data. This has the potential of developing a simple and effective method of determining case depth without resorting to a more complex AC model. Yamashita has developed the four-point DC theory for a finite length cylindrical rod in 1996 [22] and that for hollow conducting cylinders in 2006 [32]. A four-point AC model on cylinders has the advantage of using the whole set of data instead of just the low frequency DC part, and may improve the accuracy of measured case depth. The DC model would provide a useful check on the AC theory. Modeling of the AC field would be much more complex than that of the DC field though.

BIBLIOGRAPHY

[1] Y. Gotoh and N. Takahashi, "Examination of Electromagnetic Inspection of Surface Hardness: 3-D Nonlinear FEM Analysis Considering Nonuniform Permeability and Conductivity," *IEEE Trans. Magn.*, vol. 40, pp. 2673–2675, July 2004.

[2] W. D. Callister, Jr., *Materials Science and Engineering: An Introduction, 7th Edition*, John Wiley & Sons, Inc., 2007.

[3] "Key to metals," Viewed 04 April, 2008, http://www.key-to-steel.com/Articles/Art153.htm.

[4] "Heat Treatment of Tool Steel," . Uddeholm Tooling, 1999.

[5] C. C. H. Lo, E. R. Kinser, Y. Melikhov and D. C. Jiles, "Magnetic nondestructive characterization of case depth in surface-hardened steel components," *AIP Conf. Proc.*, vol. 820, part. B, pp. 1253–1260, 2006.

[6] V. Moorthy, B. A. Shaw and K. Brimble, "Testing of case depth in case carburized gear steels using magnetic barkhausen emission technique," *Mater. Eval.*, vol. 62, no. 5, pp. 523–527, May 2004.

[7] C. C. H. Lo, C. B. Scruby and G. D.W. Smith, "Dependences of magnetic Barkhausen emission and magnetoacoustic emission on the microstructure of pearlitic steel," *Res. Nondestr. Eval.*, vol. 84, no. 18, pp. 1821C1839, 2004.

[8] D. Buttle and W. Dalzell, "Case depth measurement by magnetoacoustic emission," *Eur. J. Non. Destr. Test.*, vol. 1, no. 3, pp. 118–126, 1992.

[9] F. Takeo, K. Nakajima, T. Baba, Y. Aonahata and M. Saka, "Arrangement of probes for measuring case depth by means of four-point probes," *Key Eng. Mater.*, vols. 270–273, pp. 82–88, 2004.

[10] W. Johnson and G. A. Alers, "Measurement of case depth in steel shafts using ultrasonic resonance," *Am. Soc. Mech. Eng. Appl. Mech. Div. AMD.*, vol. 188, pp. 61–67, 1994.

[11] C. Wang and A. Mandelis, "Case depth determination in heat-treated industrial steel products using photothermal radiometric interferometric phase minima," *NDT E Int*, vol. 40, no. 2, pp. 158–167, 2007.

[12] K. Pongsathaporn, P. Jenkittiyon, S. Daopiset and S. Watanasriyakul, "Case depth measurement of induction hardening using image processing," *Cailiao Rechuli Xuebao*, vol. 25, no. 5, pp. 564–566, 2004.

[13] *ASM Handbook, Volume 1 - Properties and Selection: Irons, Steels, and High Performance Alloys*, ASM International, 1990.

[14] "NDT Resource Center," Collaboration for NDT Education. Viewed 04 April, 2008. http://www.ndt-ed.org/EducationResources/CommunityCollege/MagParticle/Physics/HysteresisLoop.htm.

[15] N. A. Spaldin, *Magnetic materials: fundamentals and device applications*, Cambridge, U.K.: Cambridge Univ. Press, pp. 11, 2003.

[16] C. Chen, *Magnetism and metallugy of soft magnetic materials* , Dover Publications, pp. 106–107, 1986.

[17] N. Bowler and Y. Huang, "Model-based characterization of homogeneous metal plates by four-point alternating current potential drop measurements" *IEEE Trans. Magn.*, vol. 41, no. 6, pp. 2102–2110, 2005.

[18] S. R. Ahmed and M. Saka, "Enhancing Repeatability in the Measurement of Potential Drop using an Adjustable Four-Point-Probe Measuring System", *Res. Nondestr. Eval.*, vol. 18, no. 2, pp. 69-100, 2007.

[19] M. Yamashita and M. Masahiro, "Geometrical correction factor for semiconductor resistivity measurements by four-point probe method," *Jpn. J. Appl. Phys.*, vol. 23, no. 11, pp. 1499–1504, 1984.

[20] M. Yamashita, "Resistivity correction factor for 4-probe method on circular semiconductors - I," *Jpn. J. Appl. Phys.*, vol. 26, no. 9, pp. 1550–1554, 1987.

[21] M. Yamashita, "Resistivity correction factor for 4-probe method on circular semiconductors - II," *Jpn. J. Appl. Phys.*, vol. 27, no. 7, pp. 1317–1321, 1988.

[22] M. Yamashita, N. Toshifumi and H. Kurihara, "Resistivity correction factor for the four-point probe method on cylindrical materials," *Jpn. J. Appl. Phys.*, vol. 35, pp. 1948–1953, 1996.

[23] J. R. Bowler and N. Bowler, "Theory of four-point alternating current potential drop measurements on conductive plates," *Proc. R. Soc. A*, vol. 463, pp. 817–836, 2007.

[24] N. Bowler, "Theory of four-point alternating current potential drop measurements on a metal half-space," *J. Phys. D: Appl. Phys.*, vol. 39, no. 3, pp. 584–589, 2006.

[25] N. Bowler, "Analytical solution for the electric field in a half space conductor due to alternating current injected at the surface," *Journal of Applied Physics* vol. 95, no. 1, 2004.

[26] N. Bowler and Y. Huang, "Electrical conductivity measurement of metal plates using broadband eddy-current and four-point methods," *Meas. Sci. Technol* vol. 16, pp. 2193–2200, 2005.

[27] J. R. Bowler, Y. Huang, H. Sun, J. Brown and N. Bowler, "Alternating current potential drop measurement of the depth of case-hardening in steel rods", *submitted to IOP Publishing for peer review.*

[28] B. F. Ju, Y. Ju and M. Saka, "Fabrication of a microscopic four-point probe and its application to local conductivity measurement," *J. Micromech. Microeng.* vol. 15, no. 12, pp. 2277–2281, 2005.

[29] D. K. Schroder, *Semiconductor material and device characterization (second edition)*, Chap. 1. John Wiley and Sons, INC., 1998.

[30] Y. Huang, *Alternating current potential drop and eddy current methods for nondestructive evaluation of case depth*, Ph.D. dissertation, Iowa State University, Ames, IA, 2004.

[31] H. Sun, *Electromagnetic methods for measuring material properties of cylindrical rods and array probes for rapid flaw inspection*, Ph.D. dissertation, Iowa State University, Ames, IA, 2005.

[32] M. Yamashita, "Measuring resistivity of hollow conducting cylinders with a four-probe array," *Meas. Sci. Technol.*, vol. 17, pp. 3323–3327, 2006.